IDENTIFYING POSSIBLE HYDROLOGIC RECHARGE ZONES OF THE SANGRE DE CRISTO AQUIFER ON THE MILLIKEN RANCH IN LAS VEGAS, NM

by

IAN HAMILTON

Presented to the Faculty of the Graduate School of
The University of Texas at Arlington in Partial Fulfillment
of the Requirements
for the Degree of

MASTER OF SCIENCE IN GEOLOGY

THE UNIVERSITY OF TEXAS AT ARLINGTON
DECEMBER 2011

ACKNOWLEDGEMENTS

I would like to thank the members of my thesis committee for their continued support and guidance; Mr. Gordon Bennett, Dr. Qinhong Hu, Dr. Harry Rowe and Dr. John Wickham. These men provided scientific input and critical editing for this project. Without their invaluable insights, ideas and assistance, this thesis would not have been possible.

Thanks also go out to Dr. John Shomaker of Shomaker and Associates, Mr. Joe Zebrowski of the Forest Watershed Research Department of Highlands University and to Mr. Allen Cuttey and Mrs. Polly McCord from the New Mexico Office of the State Engineer. These New Mexico Professionals generously provided their time, data and expertise on this project. The owners of the Milliken, Barnett and Wilderspin ranches, as well as the city of Las Vegas and their water utilities staff, deserve thanks for being so welcoming and open in terms of allowing use of their resources and property in support of this project. Special thanks to Kenny Alderete, the foreman of the Milliken Ranch, for introducing the issue to me and for providing the necessary manpower and direction for sampling.

Finally, a note of thanks to the scientists that helped with the analysis of the water sampling back in Texas: Dr. Qinhong Hu, Dr. Benjamin Schwartz, Dr. Crayton Yapp and Prince Nfodzo.

November 22, 2011

ABSTRACT

IDENTIFYING POSSIBLE HYDROLOGIC RECHARGE ZONES

OF THE SANGRE DE CRISTO AQUIFER ON

THE MILLIKEN RANCH IN

LAS VEGAS, NM

Ian Hamilton, M.S.

The University of Texas at Arlington, 2011

Supervising Professor: Qinhong Hu

Groundwater at the periphery of mountain ranges in the desert southwest has its provenance in two possible sources: local or regional flow. This study sought to identify the source of deep groundwater from wells on ranches in the Hogback area west of Las Vegas, NM, an area under scrutiny as a possible source for municipal use. Surface and groundwater samples were taken in the area and analyzed for water chemistry and stable isotope ratios of deuterium and oxygen-18.

Ratio values were plotted against the Global Meteoric Water Line (GMWL) and also plotted on an interpolated map of precipitation values for the contiguous United States. The area plots on the map in the same precipitation range as Albuquerque, and the sampled waters cluster around the median value for Albuquerque precipitation presented by Yapp, 1986. Sampled values of surface water bodies fed by local precipitation were closely related to the deep groundwater well values, but were generally more negative. These results negate the

possibility of recharge from a regional flow regime, and show that groundwater sampled in the Hogback area is sourced from a local flow regime fed by the same precipitation recharging hydrological features around the Gallinas River, including the river itself, upland groundwater and the Montezuma Hot Springs. Chemical data from Piper grouping and ion plots supports this interpretation, and support the possibility that infiltration from surface water bodies is occurring.

This conclusion correlates groundwater west of the Precambrian uplift to groundwater to the east of its impermeable breccia zone. This correlation calls into question the extent and permeability of the breccia zone responsible for the Hot Springs. This study represents both the first set of stable isotope data and the first investigation of source data for groundwater in the area of Las Vegas, NM.

TABLE OF CONTENTS

LIST OF ILLUSTRATIONS

LIST OF TABLES

CHAPTER 1

INTRODUCTION

1.1 Problem

When considering the hydrology of an area, one question of critical concern is the source of the groundwater supply (Cartwright et al., 2005). Knowledge of the source allows for proper resource management in that it minimizes the possibility of water mining (IAEA) and the possibility of groundwater contamination from the source (Hunt et al., 2006). In order to mitigate this possibility, especially in semiarid areas with low matrix permeability and high fracture permeability (Barnes and Worden, 1998), studies involved in evaluating groundwater resources and investigating their development should seek to determine the groundwater's source. Using both isotopic and chemical techniques, groundwater in semi-arid areas can be traced via its flow path to its precipitation source.

The city of Las Vegas, NM has been continuously pumping wells in the Hogback area west of the city. In an effort to maximize its allotted groundwater pumping amount, the city is considering pumping from high yield wells on the Milliken Ranch in the same area. Previous studies have contributed to the understanding of the area hydrology and this study seeks to identify the source(s) of recharge to wells tapping the Sangre de Cristo aquifer.

1.2 Background

1.2.1 Flow regime

In desert mountain areas of the North American southwest, recharging wells may receive groundwater via either a local flow regime fed by infiltration from nearby precipitation and/or by a regional flow regime fed by the deep, subsurface flow of precipitation from adjacent mountains (Barnes and Worden, 1998). The combination of these two possible sources makes up the majority of recharge in semiarid catchments (Blasch and Bryson, 2007).

As precipitation infiltrates at a recharge zone, it enters a flow path that is directed toward a discharge zone. Both Figure 1 and Figure 2 are diagrams that depict flow paths from recharge zones to discharge zones. The recharge zones are characterized by downward flow away from the water table, and discharge zones are the opposite, experiencing upward flow toward or through the water table. Recharge zones occur mainly in the highlands, while discharge zones occur toward valleys/lowlands and/or at areas where the water table is very near the surface (Freeze and Cherry, 1979).

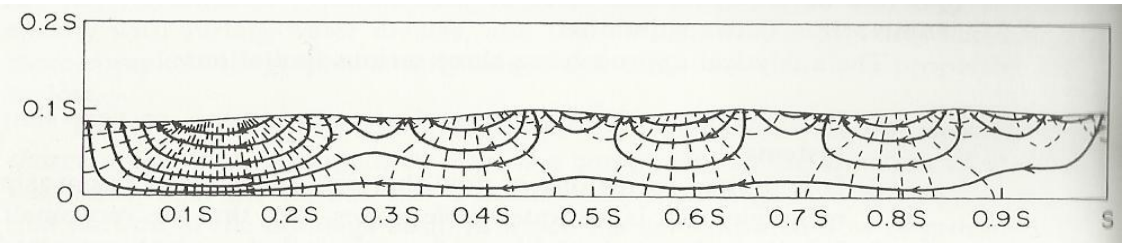

Figure 1: Diagram of groundwater moving from topographic high to low with nested flow net. Variations in topography cause hummocks in the flow net that lead to multiple flow regimes. (Freeze and Cherry, 1979)

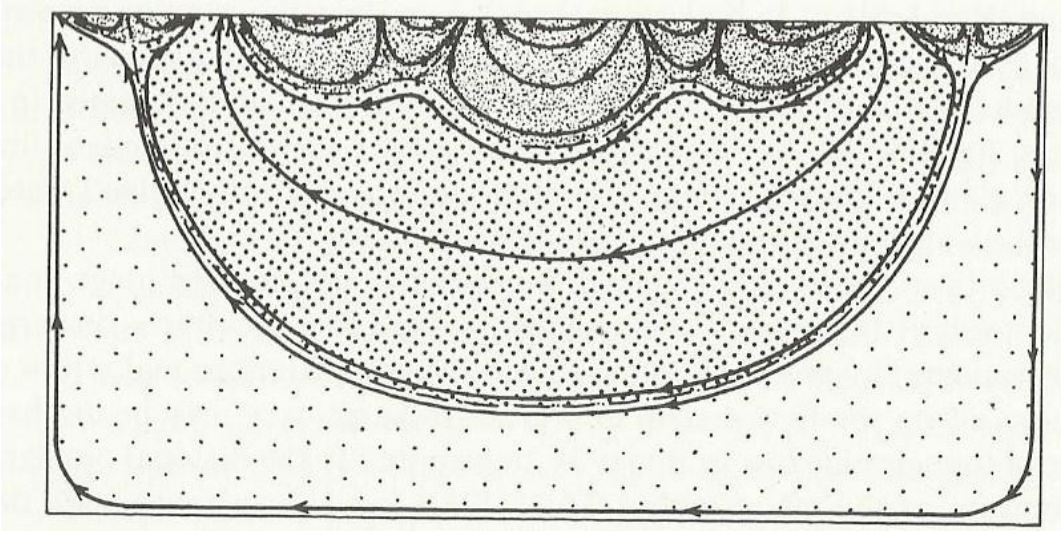

Figure 2: Diagram of a nested flow net including the three possible groundwater flow regimes: local (top, black speckled area), intermediate (middle, black dotted area), regional (bottom, sparsely dotted area). (Freeze and Cherry, 1979)

While Figures 1 and 2 demonstrate the input and output of water into a flow path, they also demonstrate how complex topography can create nested flow systems. In a local flow regime (dark, speckled areas), precipitation enters the system and flows only a short distance before reaching a discharge area. The precipitation water remains relatively shallow and water from wells tapping this flow regime will have characteristics of precipitation from the area (Freeze and Cherry, 1979).

Figures 1 and 2 also show intermediate and regional flow (dotted areas) regimes nested below the local flow loops. Precipitation entering either of these flow regimes passes deep, underneath the local flow regime. In both intermediate and regional flow, water rising from the flow path to the discharge area is a significant distance from the area of recharge. Wells tapping formations that are part of regional flow regimes may find that the groundwater sampled is more reminiscent of precipitation on land farther up the flow path than of precipitation falling locally (Freeze and Cherry, 1979).

In order to differentiate between groundwater sourced from one of the two options, two main approaches are currently in use by hydrologists: stable isotopes and ion chemistry (Aji et al., 2008).

1.2.2 Sourcing with Stable Isotopes

A largely favored method for groundwater sourcing is the use of stable isotopes as environmental tracers (Yuan et al., 2010). The stable isotope ratios of deuterium (δ^2H) and of oxygen-18 ($\delta^{18}O$) are a commonly used pair because of their stability (USGS, 2011). Assuming that no phase change or fractionation occurs along the flow path (Blasch and Bryson, 2007), stable isotope ratios of these two elements that make up water neither decay with time nor are affected by migration through most subsurface materials (Winograd and Friedman, 1972).

Water molecules contain only hydrogen and oxygen, so isotopes of these two elements make ideal tracers for water masses. These non-radioactive isotopes are stable, that is, they do not break down to form other isotopes (Eby, 2003). Deuterium is present in water at an

average proportion of 0.01%. Oxygen-18 is present in water at an average proportion of 0.2%. The abundance of the stable isotopes is a key reason that they are so relied upon for hydrology (Hem, 1985).

Stable isotope data are written in the form of a relative deviation, denoted as δ, of the heavy isotope content of a sample from that of the standard SMOW (Standard Mean Ocean Water; Craig 1961) sample. This relative deviation is determined by the following equation if 'a' denotes the absolute content of the isotope:

$$\delta = (a_{sample} - a_{standard})/a_{standard} \cdot 10^3 \text{ ‰}$$

The δ^2H is the relative deviation of deuterium, ^2H, to hydrogen,^1H, with a measuring accuracy of ±2‰. The $\delta^{18}O$ is the relative deviation of oxygen-18 to oxygen-16 with a measuring accuracy of ±0.2‰ (Dansgaard, 1964).

As mentioned above, the stable isotopes of deuterium and oxygen-18 are reliable environmental tracers because they maintain their values as they move through the subsurface. This means that groundwater stable isotope values are reflective of the precipitation values from the area of recharge (Davisson et al., 1999). Groundwater that has stable isotope ratios that are similar to local precipitation values can be inferred to be part of a local flow regime, recharged by that same local meteoric water (Mukherjee et al., 2006). On the other hand, well water with isotope values that approximate the values of precipitation from adjacent mountain blocks are inferred to be tapping an aquifer recharged by a regional flow pattern (Arnason, 1976).

Fractionation is the mechanism that causes differentiation between stable isotope values in precipitation from one area to another. When either the light or heavy isotope content decreases, the ratio decreases or increases respectively. Fractionation in water is mainly due to physical partitioning factors like evaporation and condensation, both examples of equilibrium reaction between the liquid and vapor phase (Dansgaard, 1964). Much like these two processes and phases, fractionation is highly dependent upon temperature. Therefore, factors

that affect temperature like season, altitude and latitude will also affect the fractionation of an isotope (Gat, 1996). In addition, a precipitation producing cloud preferentially rains out its heavier isotopes, causing the isotopic value of later rainfall from the cloud to lighten as it moves further inland from its oceanic moisture source. With variables like moisture source and season, the isotopic composition of precipitation in any place can not be uniform (Appendix A), so scientists rely on mean values (Eby, 2003).

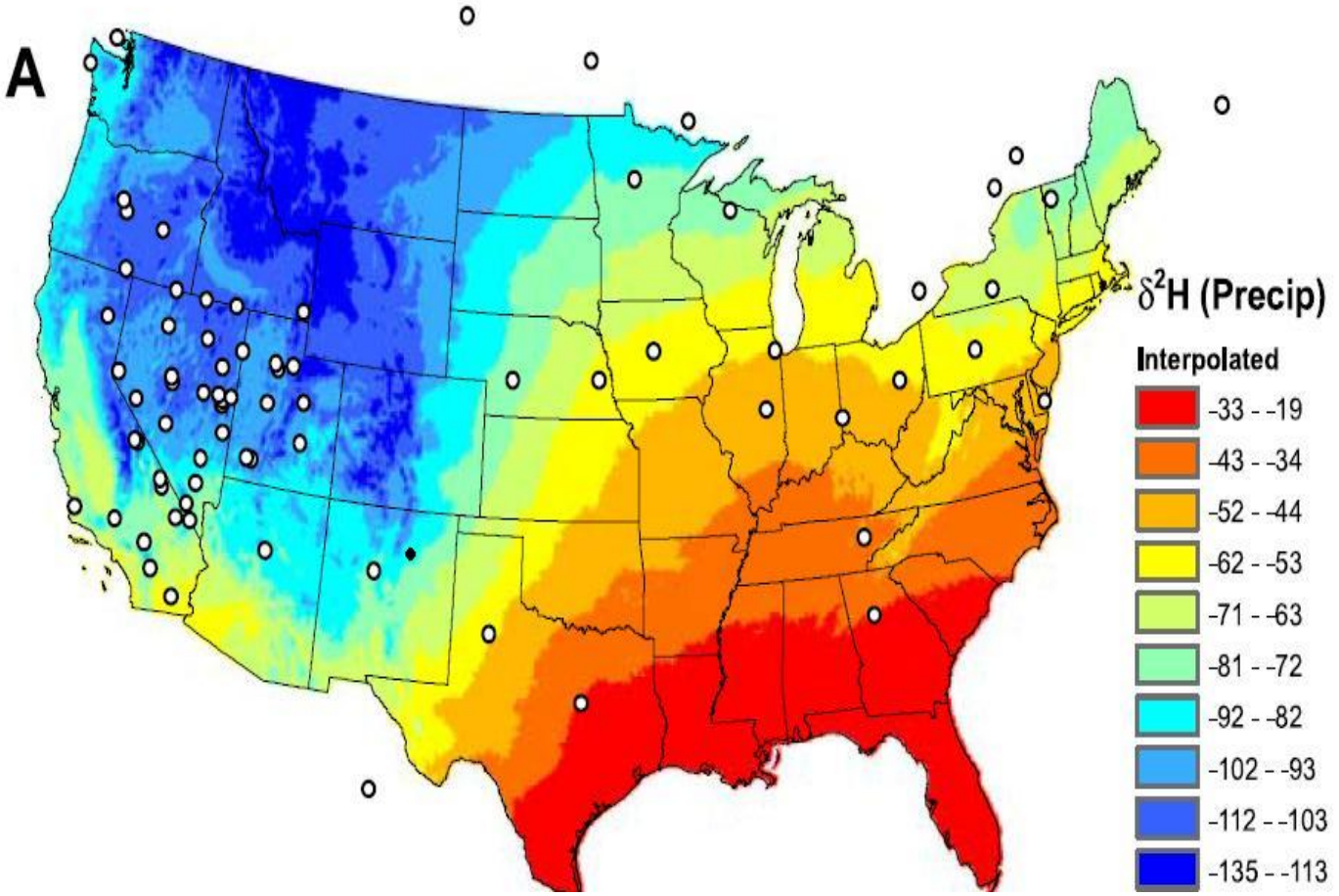

Figure 3: Interpolated map of delta deuterium values across the continental U.S. based on data from stations marked as white circles. The black circle is the thesis area near Las Vegas, NM. The white circle adjacent to it, the only other point in NM, represents Albuquerque. (Bowen et al., 2007)

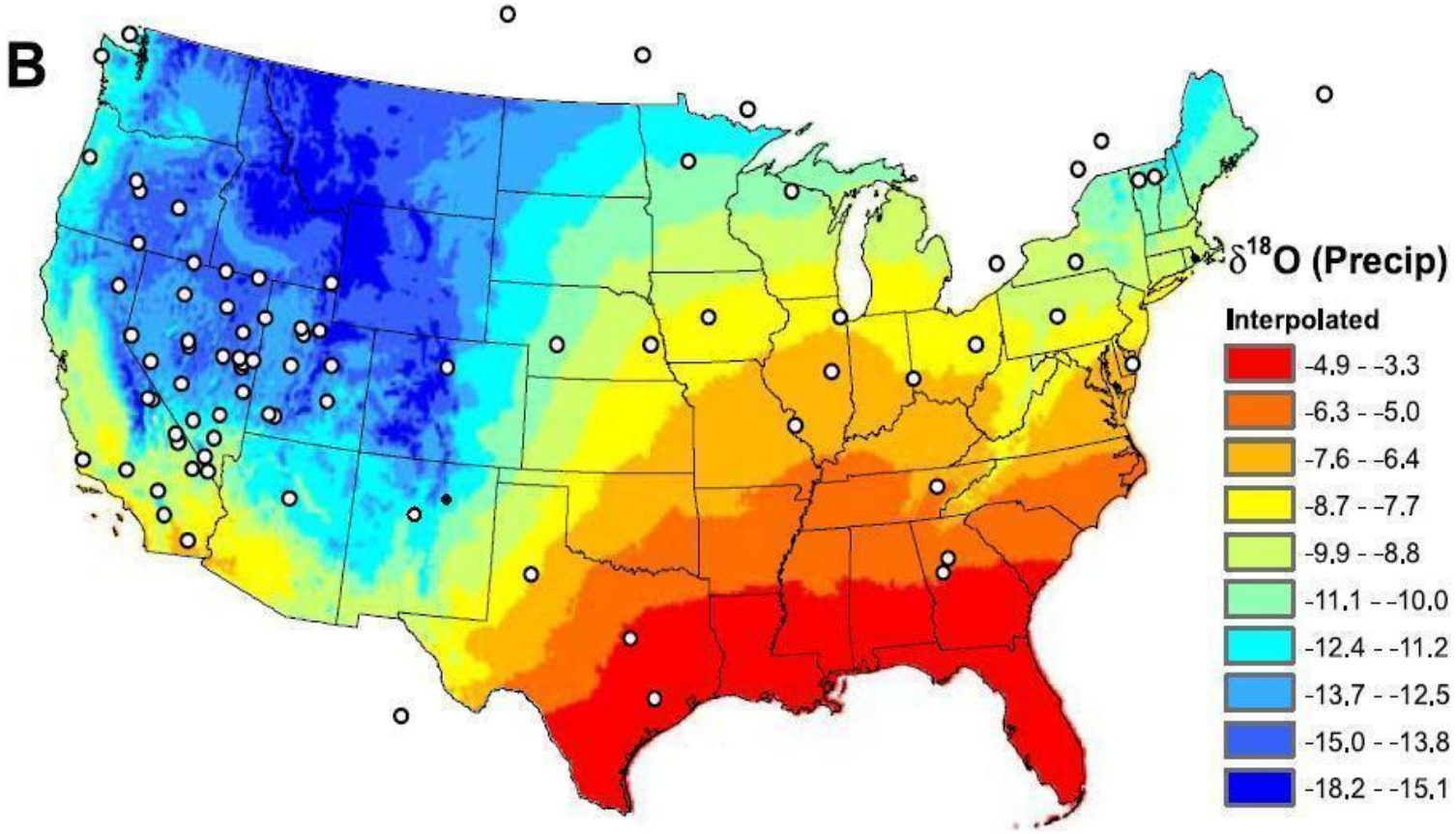

Figure 4: Interpolated map of delta oxygen-18 values across the continental U.S. based on data from stations marked as white circles. The black circle is the thesis area near Las Vegas, NM. The white circle adjacent to it, the only other point in NM, represents Albuquerque. (Bowen et al., 2007)

The IAEA (International Atomic Energy Agency) has been recording worldwide stable isotope values of precipitation since the 1960s on its Global Network of Isotopes in Precipitation (GNIP) database, and its findings have been compiled on its website for public use. Using the color coded map created by the data from this database (Bowen et al., 2007), it is possible to identify possible source areas by comparing the groundwater values from the study area to corresponding precipitation values in the region (Figures 3 and 4; Arnason, 1976). This method of sourcing groundwater recharge via precipitation maps has been used in other areas (Arnason, 1976), but this study is the first to both measure stable isotopes and to use this method in the Las Vegas area.

Since the maps are interpolated based on geographically disparate data points, they should not be considered an unquestionable resource for all precipitation data. However, they are useful because the pattern of color bands indicates the continental effect for precipitation over the Southwest. As rain producing clouds move inland from their Pacific Ocean moisture source, the heavier isotopes preferentially rain out and the stable isotope value of precipitation becomes increasingly light moving east (Wyk et al., 2011). Considering the sampled area of this study, the black dot on both maps, this pattern demonstrates that precipitation values from the thesis area should be heavier (more negative) than precipitation falling closer to the Atlantic and Gulf and lighter (more positive) than precipitation falling closer to the Pacific.

The most common method of comparing stable isotopic data is by plotting $\delta^{2}H$ vs $\delta^{18}O$ and comparing the two to the Global Meteoric Water Line (GMWL). The GMWL defines the ratio of deuterium and oxygen-18 ratios in natural, terrestrial waters, and is calculated by the equation:

$$\delta D = 8.0 * \delta^{18}O + 10‰ \text{ (Craig, 1961)}$$

Water samples that plot along the line created by the above equation are said to have come from recharge by recent precitation, as opposed to water present in the aquifer materials during deposition (USGS, 2011). Figure 5 shows an example of a plot comparing the stable isotope

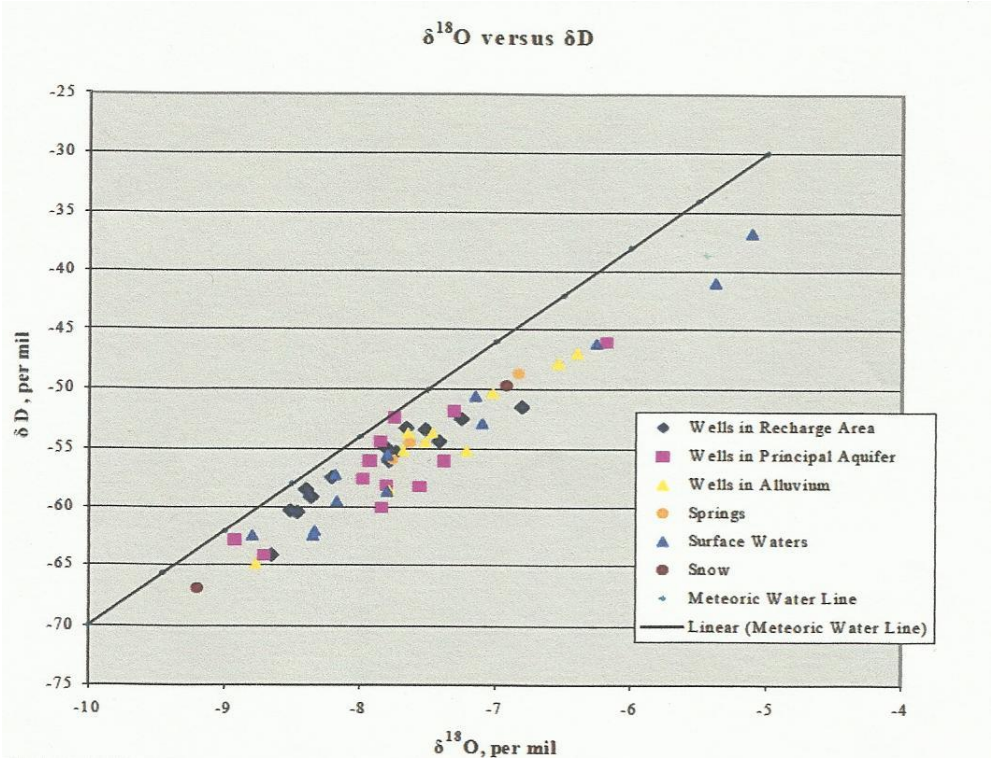

Figure 5: Example of a stable isotope oxygen-18 vs. deuterium plot against the GMWL (Gabora, 2002)

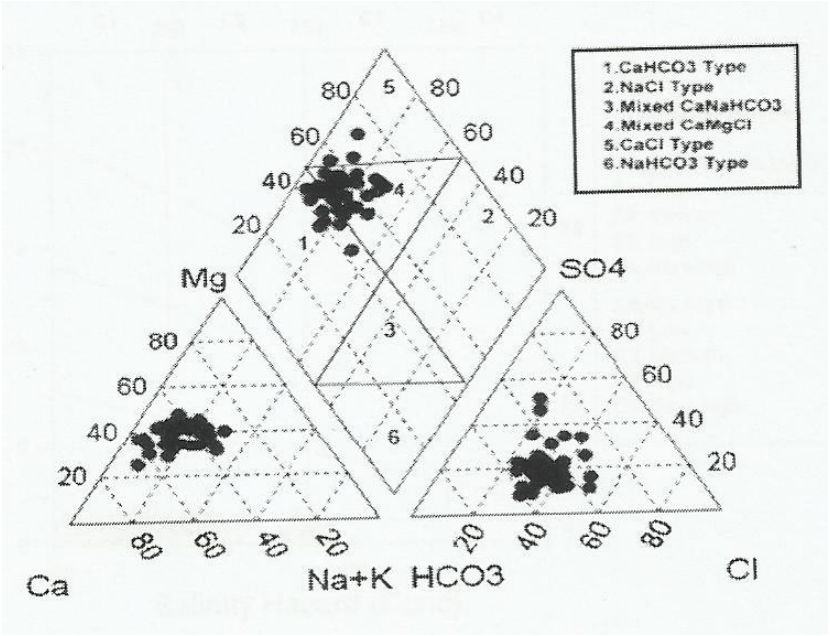

Figure 6: Example of a piper plot grouping water by ion content (Mithas, 2011)

ratios and the GMWL. Movement away from the line indicates fractionation processes like evaporation, interaction with the aquifer matrix and mixing with other waters. Placement along the line can indicate recharge source information like geography and climatic conditions (USGS, 2011).

1.2.3 Sourcing with Water Chemistry

Water chemistry is another method that has been widely used to investigate groundwater flow and sourcing. As the major ions are the most abundant dissolved constituents in environmental water, analyzing water samples for abundant cations (calcium, magnesium, sodium and potassium) and for abundant anions (chloride and sulfate) allows for grouping into chemical groups and for an understanding of water-rock interaction along the flow path (Yidana et al., 2011).

1.2.3.1 Piper Plots

Trilinear diagrams are in common use in the geological sciences, and the Piper plot is a common method for water analysis interpretation. Two trilinear plots with data from the major anion and cation concentrations are combined into a diamond plot that may demonstrate relationships between samples. These relationships include mixing, downslope interaction trends and salt effects (Lakshmanan et al., 2003).

Figure 6 shows an example of a Piper diagram with plots for water samples. The diamond is split into four individual diamonds, and assigns water samples to one of four groups based on their ionic chemistry. If plotted in the top diamond, the water is grouped as Ca-Mg-SO_4-Cl type. The left diamond holds water of the Na-K-SO_4-Cl type. The bottom diamond is where water is of the Na-K-HCO_3 type, and the right diamond is for water of the Ca-Mg-HCO_3 group. Assigning water types to samples allows analysis of mixing and change with water movement down the flow path and with depth (Grassi et al., 2011).

1.2.3.2 Ion Plots

As water interacts with minerals in the rock, ion exchange processes change the water's chemistry. The effects of these interactions should increase with distance from the source, and can support hypotheses about flow and recharge direction (Lingjuan, 2011). Scientists have noticed that dissolved solids concentrations, which represent the amount of dissolved ions in solution, are typically lower near recharge sources. As residence time and interaction with subsurface minerals increase with flow through the aquifer, concentrations of total ions increase (USGS, 2011).

Spatially comparing cation to anion concentrations reveals specific exchange reactions occurring between water and minerals. These comparisons can indicate which formations and minerals are reacting the most with the groundwater (Petitta et al., 2010). An increase of sodium, for instance, indicates interaction with clays, while a decrease in sulfate indicates sulfate reduction and interaction with coals and carbonaceous shales. These comparisons can also help to establish the existence of dual groundwater regimes: regional deep and shallow local. The following are the possible conclusions for the trends of major ion compositions as groundwater flows away from its source (USGS, 2011):

1. Increase in Na^+ and SO_4^{2-} → Shallow, local
2. Increase in Na^+ and decrease in SO_4^{2-} → Mixing between shallow and deep
3. Decrease in Na^+ and decrease in SO_4^{2-} → Regional, deep

1.3 Goals and Objectives

The goal of this research was to ascertain the source of groundwater in ranch wells in the Hogback area west of Las Vegas, NM. The results of this research will provide insight into the hydrology of the Las Vegas area and provide an initial set of stable isotope data for follow-up studies. Specific objectives of this research include the following:

1. Compare sampled δ values to precipitation map for possible regional source

2. Correlate ranch groundwater to surface water up gradient using stable isotopes and water chemistry for possible local source
3. Assess change with distance from surface water bodies for possible infiltration

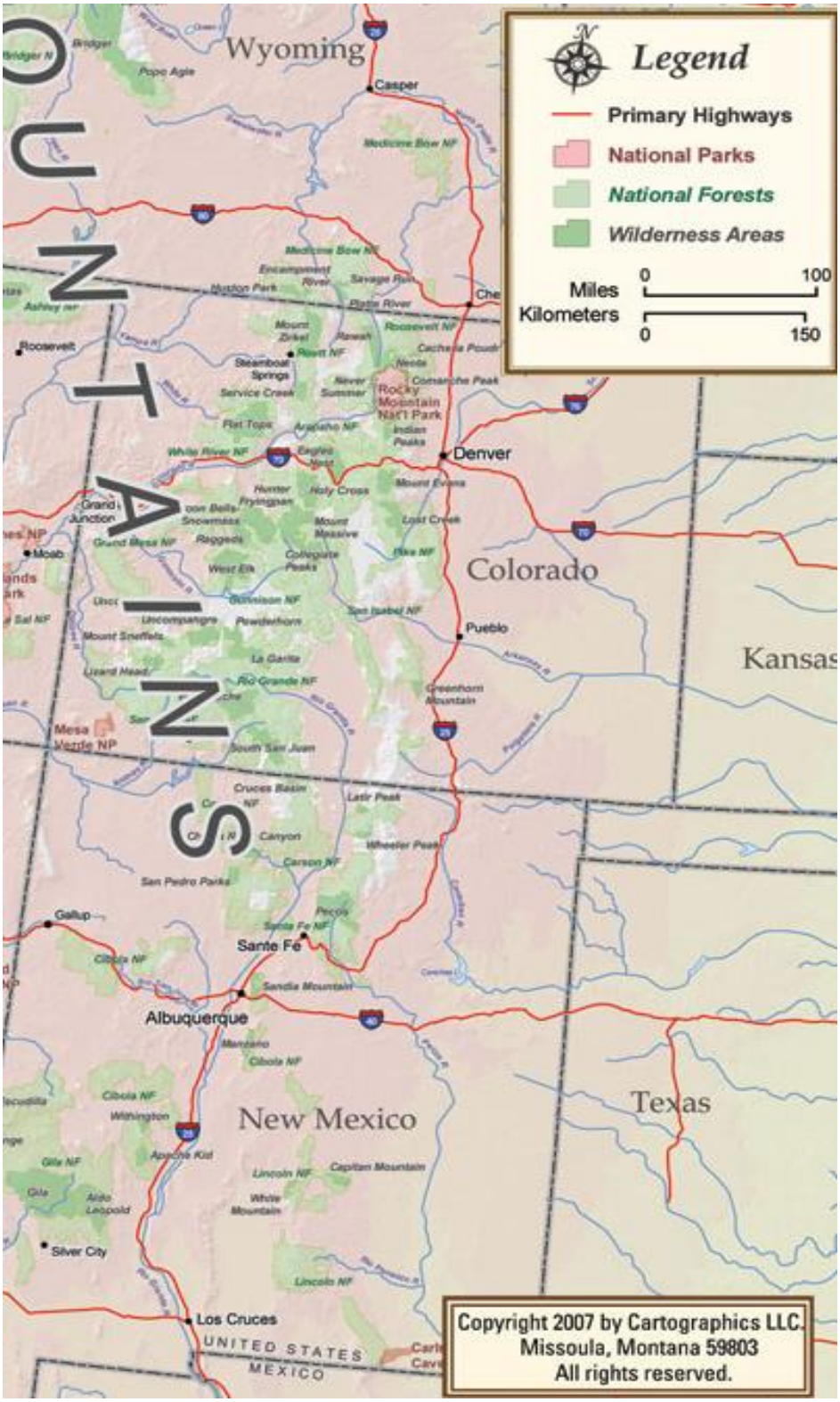

Figure 7: Map of Southern Rocky Mountain Sub-region of the Rocky Mountain System.

1.4 Study area

1.4.1 Location

1.4.1.1 Regional

References to the region of the study refer to the area that receives precipitation capable of initiating/entering a possible deep flow regime that will flow beneath the local flow regime in the sampling area west of Las Vegas, NM. The region is known as the Southern Rocky Mountain sub-region, and is located in the American West; it is also commonly referred to as the Colorado Rockies. Although ~60% of the mountains are located in Colorado, ~20% spills over into Wyoming and ~20% down into New Mexico. Centered at 38° 56' N; 106° 34' W, it extends 542 miles north-south and 255 miles east-west, covering an area of 79,008 sq. mi (peakbagger.com). Figure 7 shows a map view with state lines, interstates, rivers and nationally protected areas of the Southern Rocky Mountain sub-region.

1.4.3.2 Local

The study area, referred to as the Hogback area in this paper, is situated principally in the Ojitos Frios quadrangle of north-central New Mexico. The Hogback area refers to the area that was sampled; it lies just west of the city of Las Vegas, the seat of San Miguel County (Figures 8 and 9), and includes the cities of Montezuma and Hot Springs, as well. Bounded by eastings 473000 and 479000, and northings 3935000 and 3946000, the Hogback area is approximately 12 sq. mi (Figure 10). Of principal interest in this study are the well fields on the Taylor, Milliken and Wilderspin ranches and the surface waters north of these fields: the Montezuma Hot Springs, the Gallinas River and the reservoirs that receive diversions for municipal use (Figure 10). These two reservoirs, the Bradner and the Peterson, lie due north of the sampled well fields. Excessive diversion of this river is a major factor driving the search for additional water sources for the population of the three cities and their surrounding suburbs, an accumulated population of around 15,000 (Figure 11).

The area purported to be responsible for local flow encompasses a larger area. The headwaters of the Gallinas at the summit of Elk Mountain are the westernmost boundary, and its entire watershed until the interface between the mountains and the plateau is the eastern boundary (Figure 9).

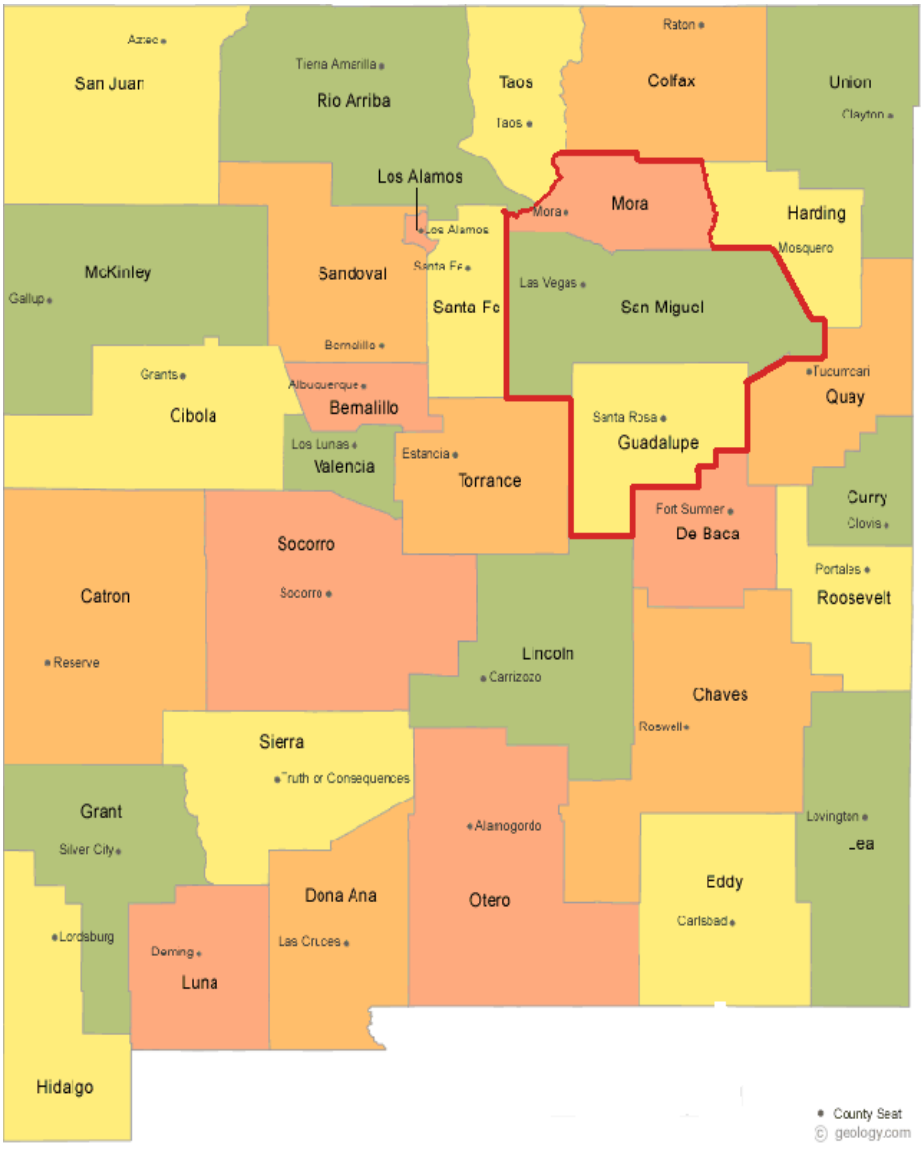

Figure 8: New Mexico County Map from Geology.com. Grey dots represent the county seat: Las Vegas is the county seat of San Miguel County. The Upper Pecos River is situated within the three counties bordered in red, as seen in Figure 9.

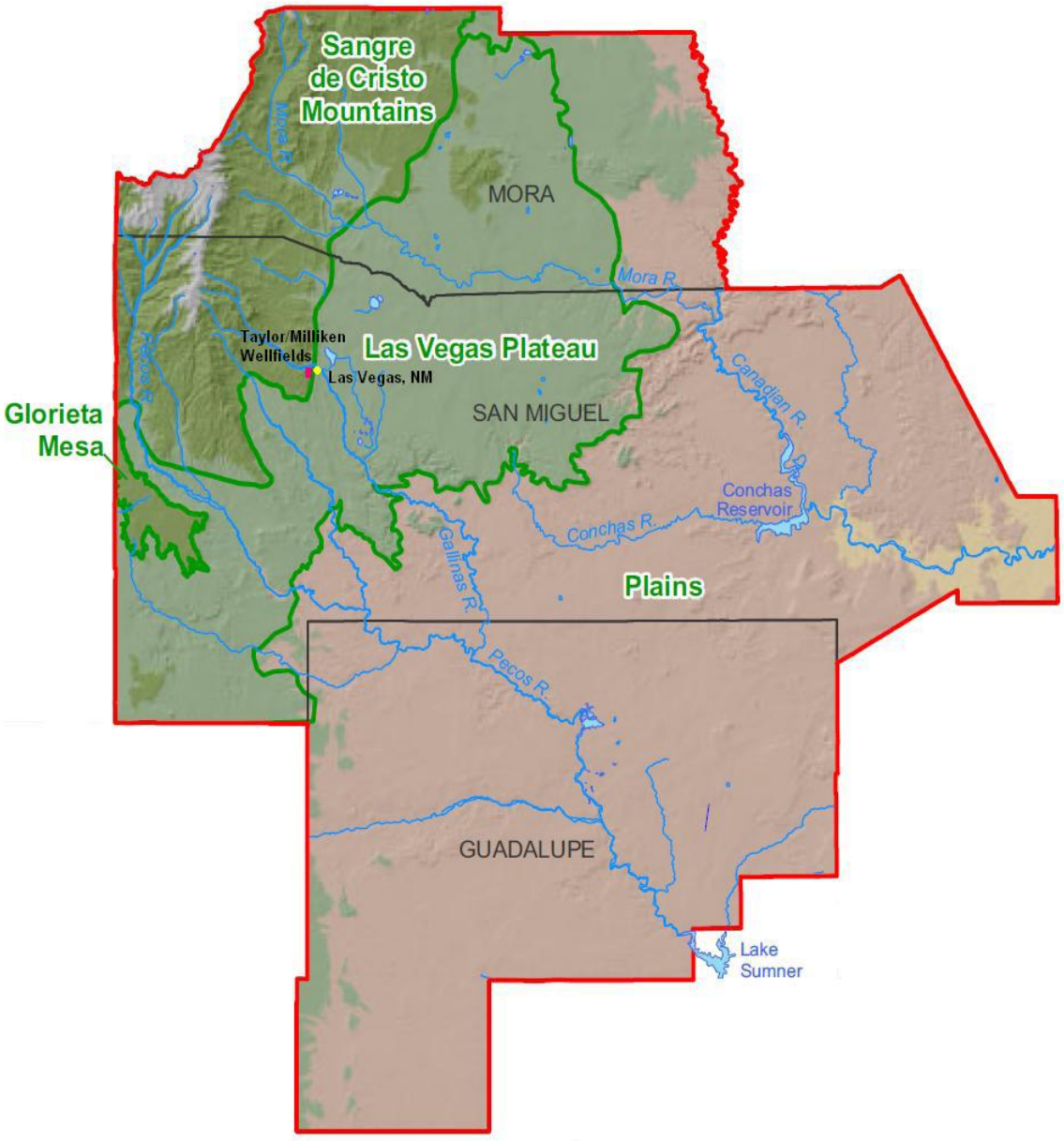

Figure 9: Tricounty area containing the Pecos River. The Gallinas River feeds into the Pecos. Las Vegas lies on the Gallinas River near its source, and is shown as a yellow dot. Just west is the Hogback Area, shown as a pink rectangle. The two lie at the border of the Sangre de Cristo Mountains and the Las Vegas Plateau. (City of Las Vegas, 2010).

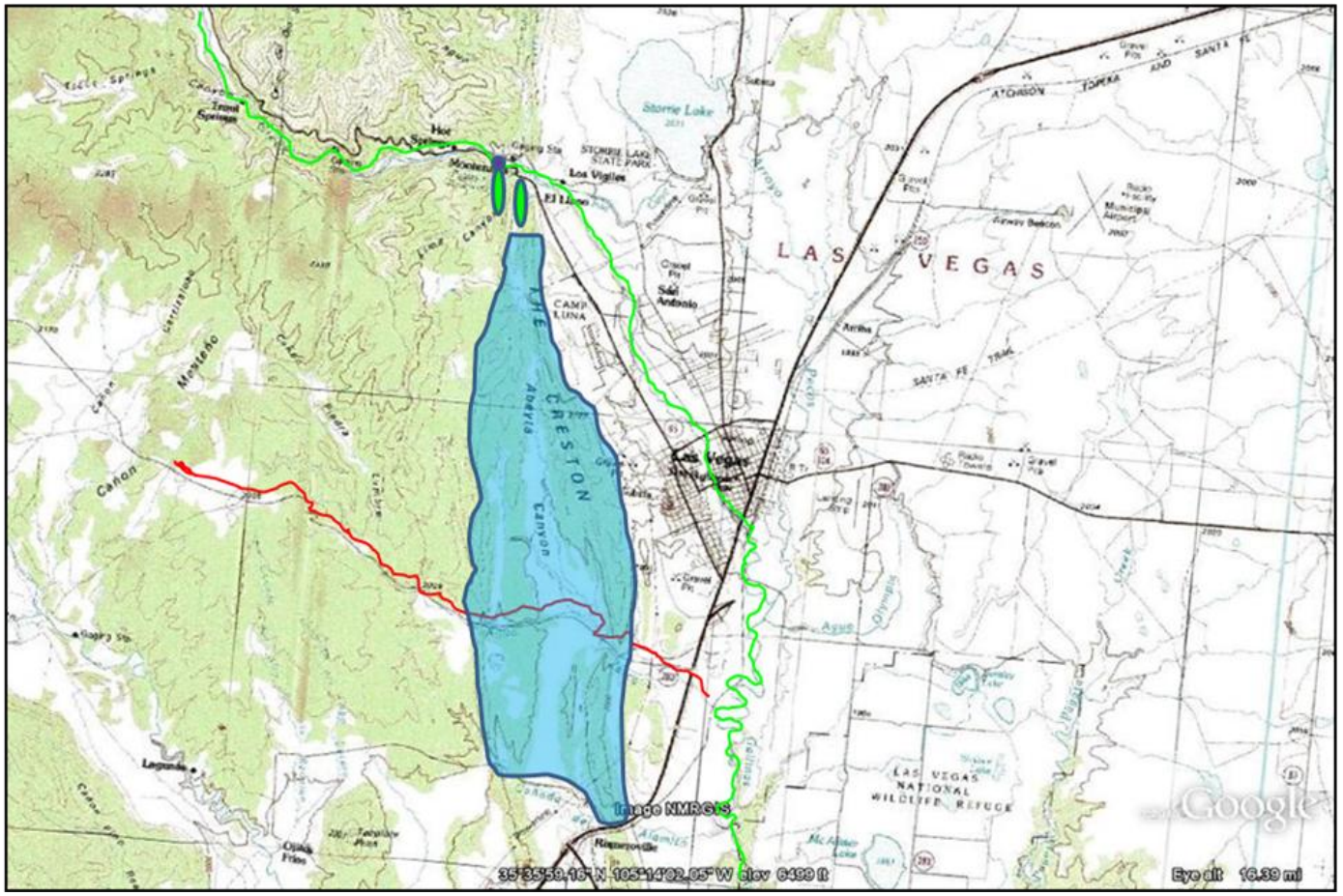

Figure 10: Thesis area topography map at the junction of four USGS quadrangles: Ojitos Frios, Montezuma, Las Vegas and Las Vegas NW. The Hot Springs is marked as a purple circle. The Bradner and Peterson reservoirs are marked as lime green ovals. The Gallinas River is marked as a lime green line. The Agua Zarca stream is marked as a red line. The ranches are marked as transparent, blue polygons.

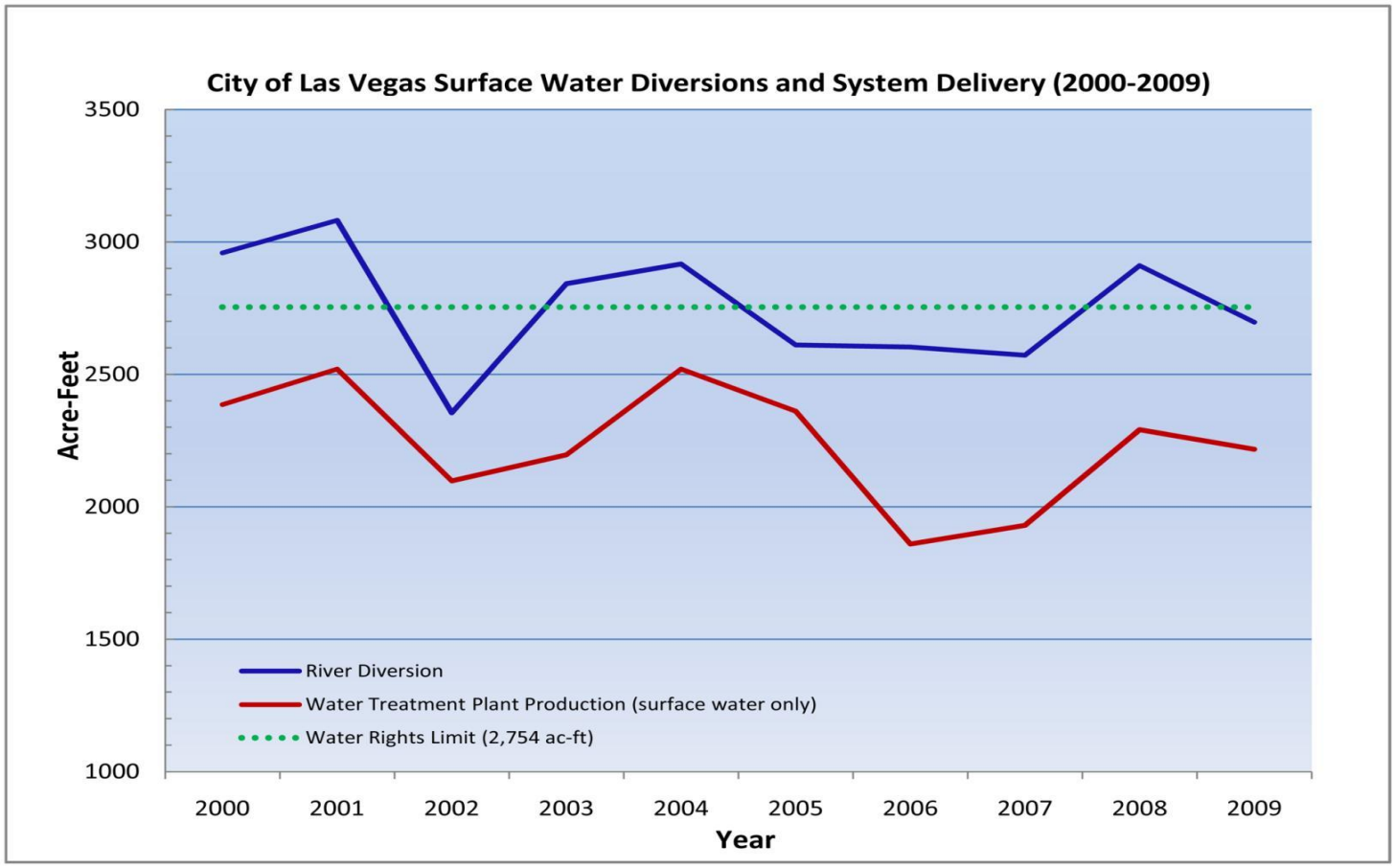

Figure 11: Graph of Las Vegas use of the Gallinas River against the allotted limit from the OSE. (City of Las Vegas, 2010)

1.4.2 Physiography

1.4.2.1 Regional

The areas of regional recharge occur on the sub-ranges of the Southern Rocky Mountain sub-region of the Rocky Mountain system. The sub-ranges included are the Sangre de Cristo Range, the San Juan Mountains, the Central Colorado Range, the Sawatch Range, the Elk Range Area, the Front Range, the Flat Tops Area, the Southern Wyoming Range and the Park Range. The Southern Rocky Mountains have many tall summits, including all thirty of the highest peaks in the Rockies. Three major basins, the San Luis, the Albuquerque, and the Espanola, separate several of the sub-ranges, creating high relief in the area (Tweto, 1975).

1.4.2.2 Local

The high yield well fields involved in this study are located on the ranches that are situated between two hogbacks that continue north-south along the entirety of the Ojitos Frios quadrangle (Figure 10). The easternmost hogback is known as the Creston. It marks the eastern perimeter of the Sangre de Cristo Mountains before the topography transitions into the Las Vegas Plateau. Moving westward from the Creston, the topography falls to a low known as Abeyta Canyon. The canyon gradually grades upward 100 feet in elevation, an intermediate rise that falls again into a narrow valley. This narrow valley is bound to the west by the westernmost hogback, the Glorieta ridge. Directly adjacent to this ridge is a third, thin valley that, along with the other two valleys, drains into the Agua Zarca ephemeral stream. This stream cuts through both hogbacks along Highway 283 until it empties into the Gallinas River south of the city of Las Vegas. To the northwest of the city, the distance between the two hogbacks decreases until they reach the Gallinas River's eastern flow path. Just south of the river, before it escapes the Sangre de Cristo Mountains, the city of Las Vegas maintains two reservoirs for municipal use. The Peterson reservoir lies in the valley west of the Glorieta ridge and the Bradner reservoir lies in the valley between the two converging ridges. On the north

side of this section of the Gallinas River are the Montezuma Hot Springs, which emerge just feet from the channel banks (Figure 10).

The Gallinas watershed is ~52,000 acres in area and is sandwiched between the Rio Grande Watershed and the Canadian River Watershed. The main section of interest as the recharge source for local flow is the northwest corner of the watershed, which is entirely within the Sangre de Cristo Mountains. The river maintains a southeasterly course, following the topography changes of the mountain range (Kaysing, 2006).

1.4.3 Geology

1.4.3.1 Regional

The Rocky Mountains are located in the Laramide region, meaning that they were created by uplifts related to northeast-southwest shortening effects of the flat subduction of the Farallon plate between 80 and 40 Ma (Fan et al., 2011). The area maintains a high percentage of Precambrian basement exposure from uplift events during the Late Cretaceous period and the early Cenozoic era. The many uplifts created numerous reverse faults, resulting in basins that hosted sedimentary deposition (Fan et al., 2011). A post orogenic epeirogenic swelling uplifted the mountains even more, setting the Southern Rocky Mountains apart from other mountain chains in terms of elevation. This epeirogeny was created partly by lithospheric thinning and crustal thickening and partly by excessive stream incision during the Miocene climate change. The epeirogenic swell lifted everything upon it, including the basins and Great Plains that jut against the mountains (Eaton, 2008). The Piedmont slope, for example, is shown on Figure 11 as the top line, the line that begins at the highest elevation. Its profile provides a much higher gradient and elevation change, a complex system that leads to regional flow regimes. Figure 12 shows a smoothed topographic map of the area. The existence of the epeirogenic swelling is evident by the elliposoidal contour lines with the highest elevation in the middle and subsequent, concentrically lowering elevations in all directions. This isostatic

adjustment explains how the region is able to act as the source of stream channels that flow in every direction but north (Eaton, 2008).

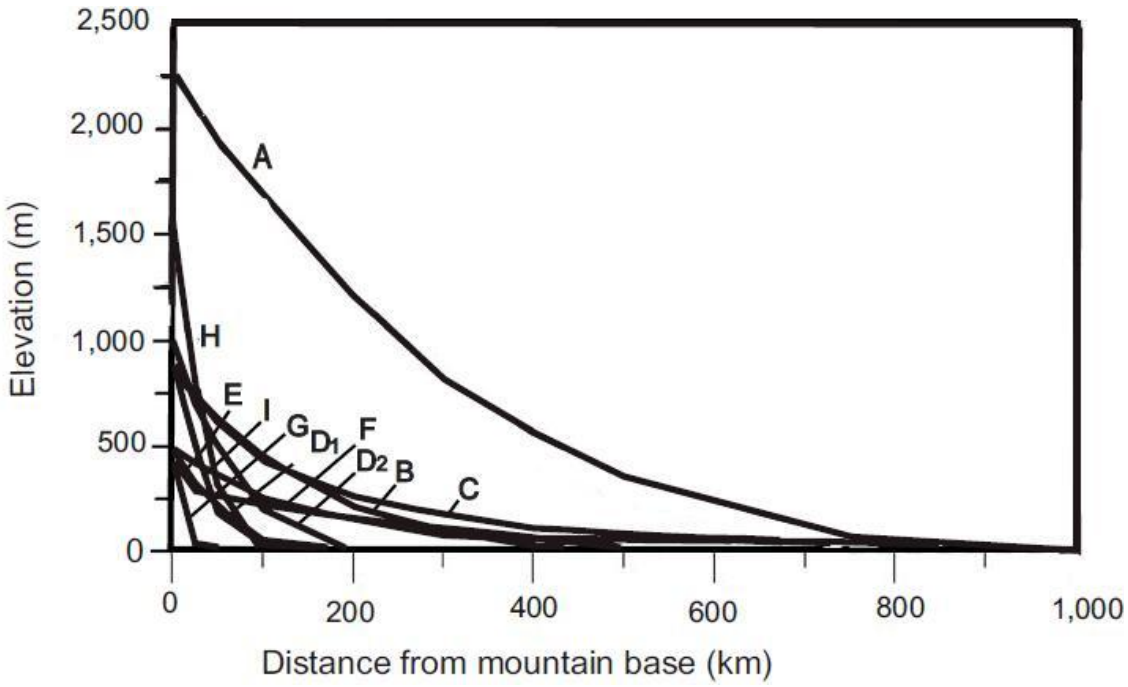

Figure 12: Profiles of piedmont slopes of major mountain ranges of the world. Profile labels are as follows: A - Southern Rocky Mountains; B - Alps; C - Atlas; D - Andes; E - Pyrenees; F - Himalayas; G - Caucasus; H - Wrangell Mtns.; I - Alaska Range. (Eaton, 2008)

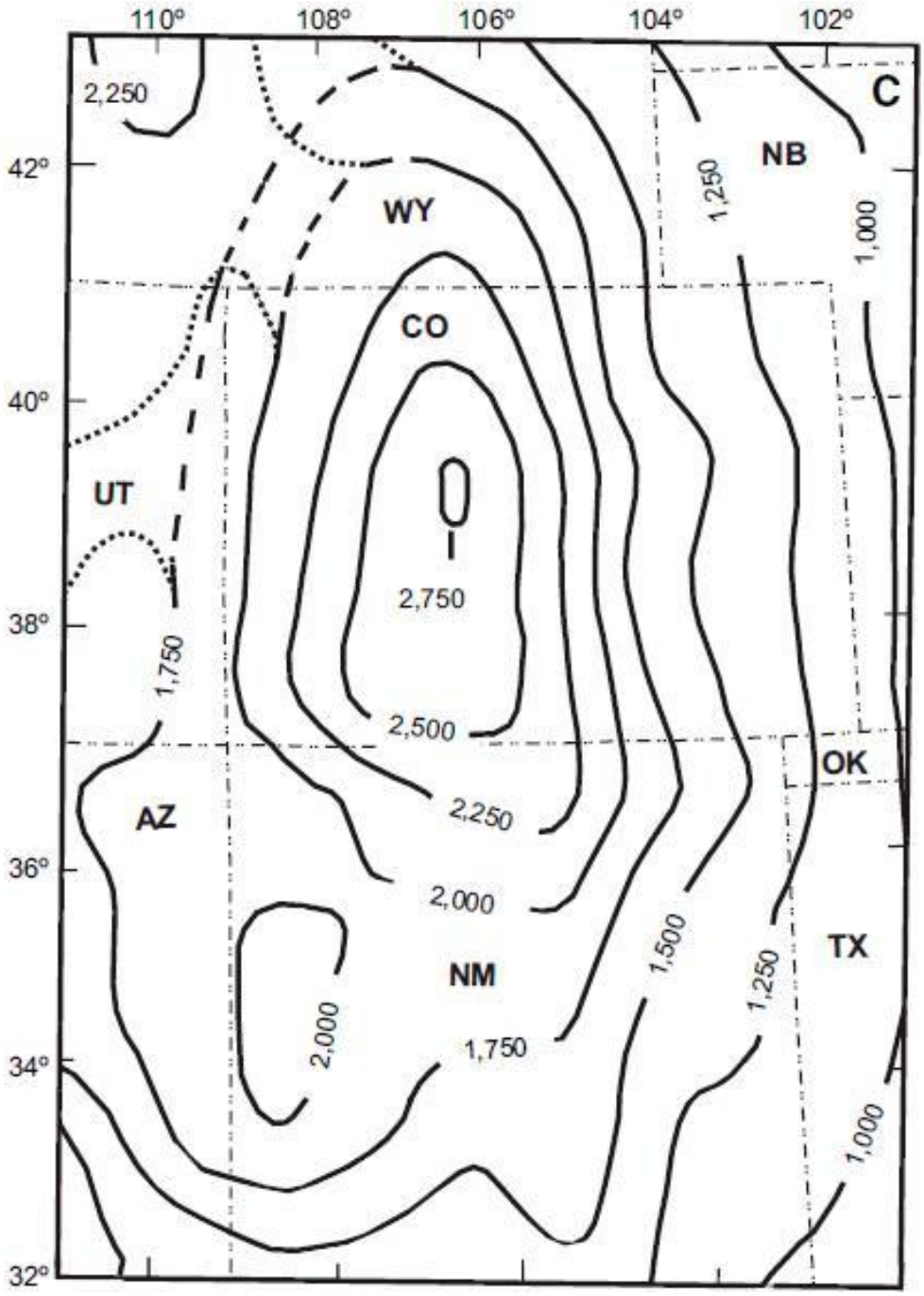

Figure 13: Smoothed topographic map (250 m contour interval) of the summit region of the Southern Rocky Mountain epeirogen and its surroundings. (Eaton, 2008)

1.4.3.2 Local

The Hogback area is located at the eastern edge of the Sangre de Cristo Mountains at their interface with the Las Vegas Plateau at a North-South trending syncline (Figure 9). The area is the result of extensive compressional forces that came from the west (Griggs and Hendrickson, 1951). The earliest structure that was developed was the thick Precambrian metasedimentary rocks that underlie all the strata of the area. Their presence signifies that the area was part of a sub-basin, accepting sediment until the Laramide orogeny. The orogeny formed the Las Vegas syncline, which is asymmetrical with an overturned western limb in the area of Las Vegas (Lessard and Bejnar, 1976). A rough pictorial representation of the formation of the syncline is shown on Figure 14 from Bejnar and Bejnar, 1979. The position of the western limb exposed outcrops of the earlier deposited sedimentary layers to the surface, so the dip of formations that underlie the Hogback area are between 50 and 90 degrees (Figure 15). The exposition of these raised sedimentary layers created topography conditional to the resistance of the stratigraphic lithology. A brief stratigraphic column appears in Appendix B.

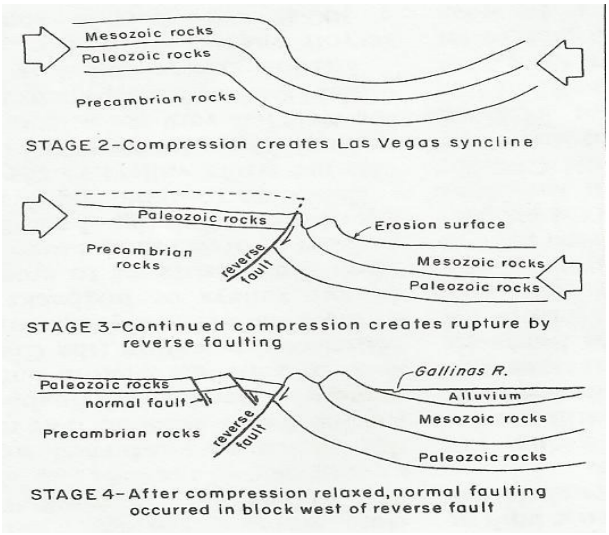

Figure 14: Developmental cross section of Creston Area with respect to the formation of the Las Vegas syncline. Stage 1, the deposition of the Mesozoic and Paleozoic rocks, is not included. (B and B, 1979)

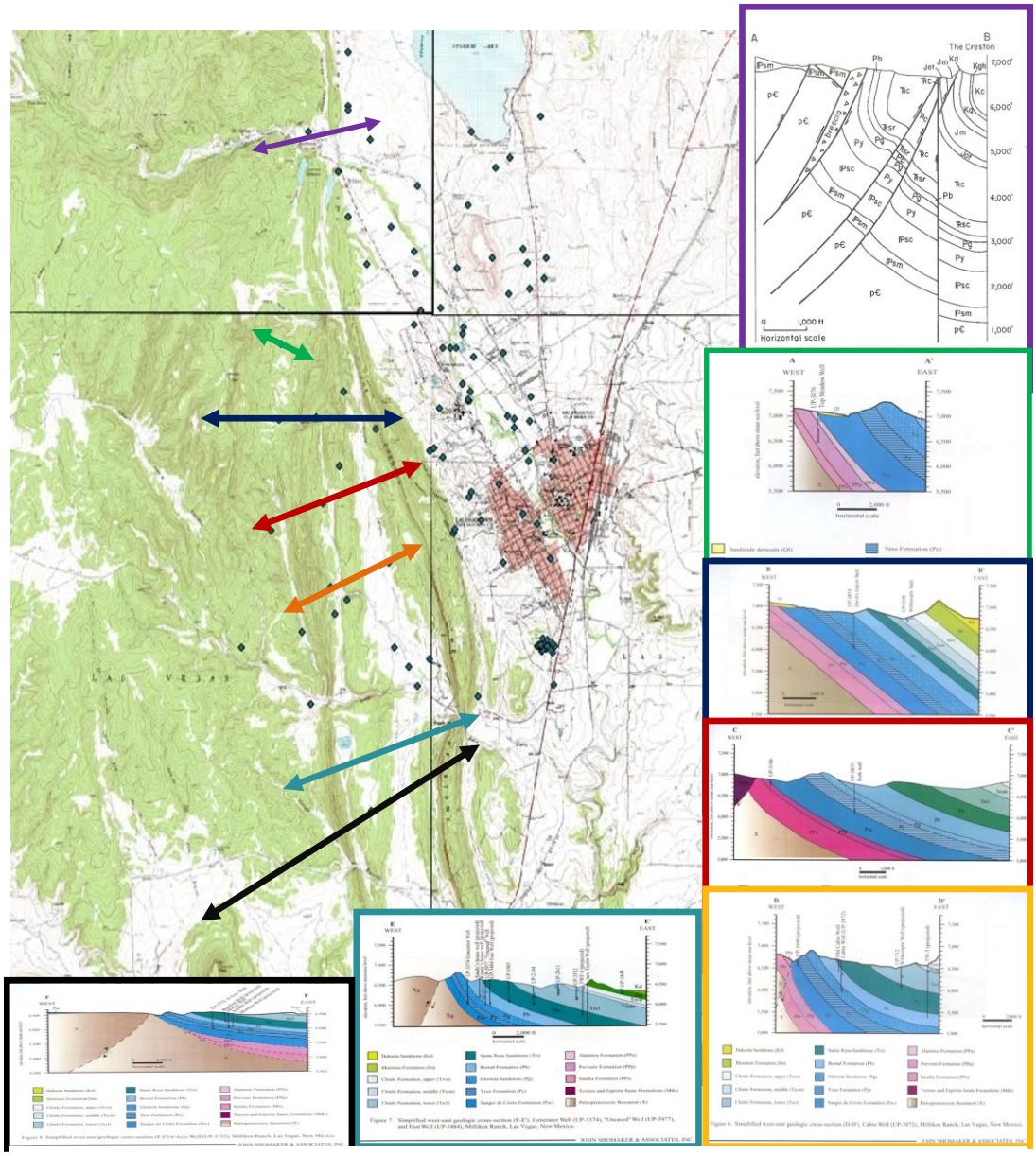

Figure 15: Topographic map of local study area with cross sections along length of ranch areas and hot springs. (Bejnar and Bejnar, 1979; Shomaker, 2007)

Consistent with the structure of the syncline, the layers slope east toward the axis of the fold with dips that range from vertical to 45° (Figure 15). Continued compression following the Laramide orogeny created a series of faults and fractures west of the resulting basin, the first occurring at the eastern most hogback, known as the Creston. This fault is known as the Montezuma fault, a reverse fault that follows the Creston along its north-south trajectory. Further compression created a succession of normal faults, including one along the Glorieta hogback that uplifts the Precambrian metamorphic basement to the surface (Griggs and Hendrickson, 1951). The effects of faulting can be seen along the two fault-ridden hogbacks in the form of fractures, offsets and breccia zones (Figure 16). The breccia zone occurring within the study area underlies the Peterson Reservoir, which occurs to the west of the Glorieta hogback between the Gallinas River and the Gallinas Canyon (Bejnar and Bejnar, 1979).

According to Bejnar and Bejnar, 1979, the fractures, faults, offsets and breccia zone work together to create the conditions that led to the formation of the Montezuma Hot Springs. The uplift of the metasedimentary basement rock allows for local percolation of local meteoric water. The water attains geothermal heat from three possible sources: an abnormally high geothermal gradient, original heat from Precambrian rocks, and subsurface magma related to ancient volcanism (Bejnar and Bejnar, 1979). This heated water trickles through fractures and flows east toward the Las Vegas Plateau until it encounters the breccia zone at the Peterson Reservoir fault. This 300 ft. wide breccia zone developed along this 2000-ft-throw reverse fault and acts as an impermeable dam, accumulating and ramping groundwater to the surface before the temperature cools (Figure 16, Bejnar and Bejnar, 1979).

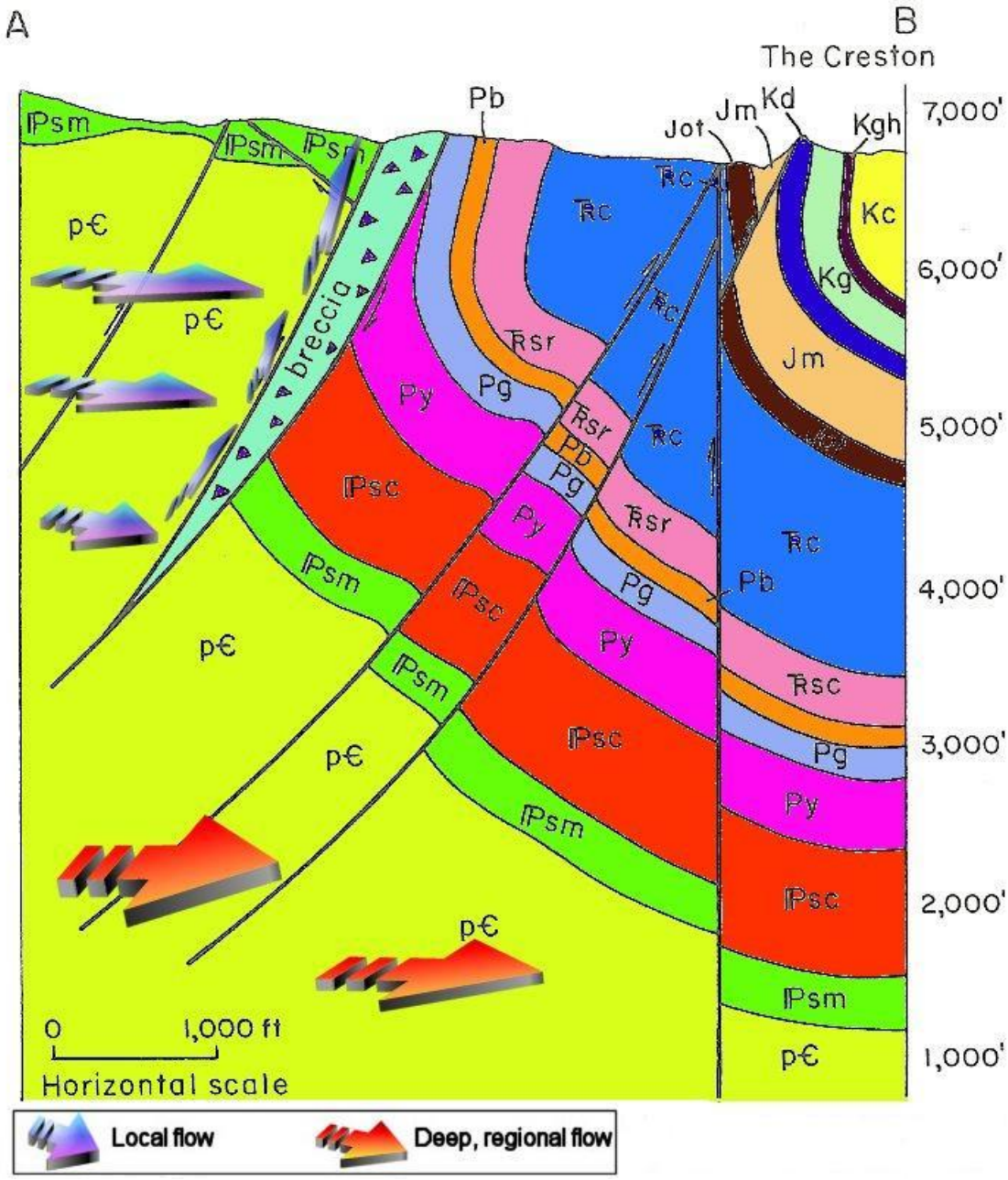

Figure 16: Zoomed in cross section of purple arrow (top arrow) from Figure 15. Shows major faults, breccia zones, formations and flow regime possibilities. See Appendix B for lithologic key. (Bejnar and Bejnar, 1979)

1.4.4 Hydrology

1.4.4.1 Regional

1.4.4.1.1 Atmosphere

The climate of the sub-region varies by season, but is mainly characterized by low humidity and abundant sunshine, especially around Colorado's highlands. Winters are generally cold and snowy, especially in the higher elevations of the Rocky Mountains. Summers are characterized by warm, dry days and cool nights. The average annual temperature at high elevations is ~0°C, but normal temperatures range from -9 to 6°C. High altitude areas receive the largest amount of annual precipitation, mainly in snowfall, where it ranges from 7 to 25 inches (peakbagger.com).

1.4.4.1.2 Surface Water

Many rivers originate from the snow melt of the Southern Rocky Mountains (Figure 7). Those in the northern part of the sub-region, most notably the Arkansas River, are part of the western boundary of the Missisippi River drainage basin. Those in the southern part of the sub-region are at the northern edge of the Rio Grande drainage basin. The Rio Grande River originates in the Southern Rocky Mountains at Colorado and passes through them along the Rio Grande Rift until veering east to empty into the Gulf of Mexico. Water draining off the western parts of the Southern Rocky Mountains empties into the Colorado for drainage into the Gulf of California; the sub-region is the boundary for several of the largest drainage basins in North America.

1.4.4.1.3 Groundwater

Substantial groundwater infiltration exists at high altitude throughout the Southern Rocky Mountain sub-region as evidenced by groundwater levels from the Colorado Division of Water Resources, 2011. As mentioned above, the high temperatures in summer keep glaciations and other natural barriers to infiltration at bay (peak-bagger.com). This characteristic, along with high volumes of precipitation, ensures that groundwater supplies are

constantly recharged at these high altitude zones. The water must enter the system through secondary porosity, and will penetrate deep into the geology because of the high relief. This deeply penetrating water will create both local and regional flow regimes that will follow the direction of flow for a very long distance (Tweed et al., 2009).

1.4.4.1.4 Flow direction

The Southern Rocky Mountains act as a surface water divide on the North American continent, so flow direction can be segregated into flow on one side of the mountains versus flow on the other side. Channels emanating from mountains in the northeast of the subregion flow east toward the Mississippi. Those on the western side of the mountains flow southwest toward the Pacific Ocean. Those in the southern side of the Southern Rockies flow southeast toward the Gulf of Mexico.

Groundwater very often follows topography in terms of flow direction, so the aquifer water is expected to flow in the same directions as above. The recharge zone for groundwater in these districts must come from infiltration at the highest points of the mountains. The ultimate destination of this high altitude recharge groundwater is likely into the major channels that emanate from the same area. Mountain recharge groundwater in this sub-region likely has its discharge area at adjacent, low altitude basin areas.

1.4.4.2 Local

1.4.4.2.1 Atmosphere

The Ojitos Frios quadrangle in the Northeastern region of New Mexico near Las Vegas lies at the frontier between the Sangre de Cristo Mountains and the Las Vegas Plateau (Figure 9), so the area experiences conditions that characterize both the desert plains and mountains. The average temperature is overwhelmingly moderate, but this does not reflect the daily temperature flux that accompanies the presence and absence of the sun (Figure 17). The rainfall is scarce in this area, ranging from 15 to 18 inches per year, with the wettest season occurring during the summer months (Figure 17). Snow falls regularly during the winter months,

averaging near 40 inches, but the average snow cover does not exceed one inch due to a very high evapotranspiration rate, ~53 inches (Appendix C). This not only affects the precipitation, but also the surface water draining from the higher elevation snowmelt (Aguirre, 2009).

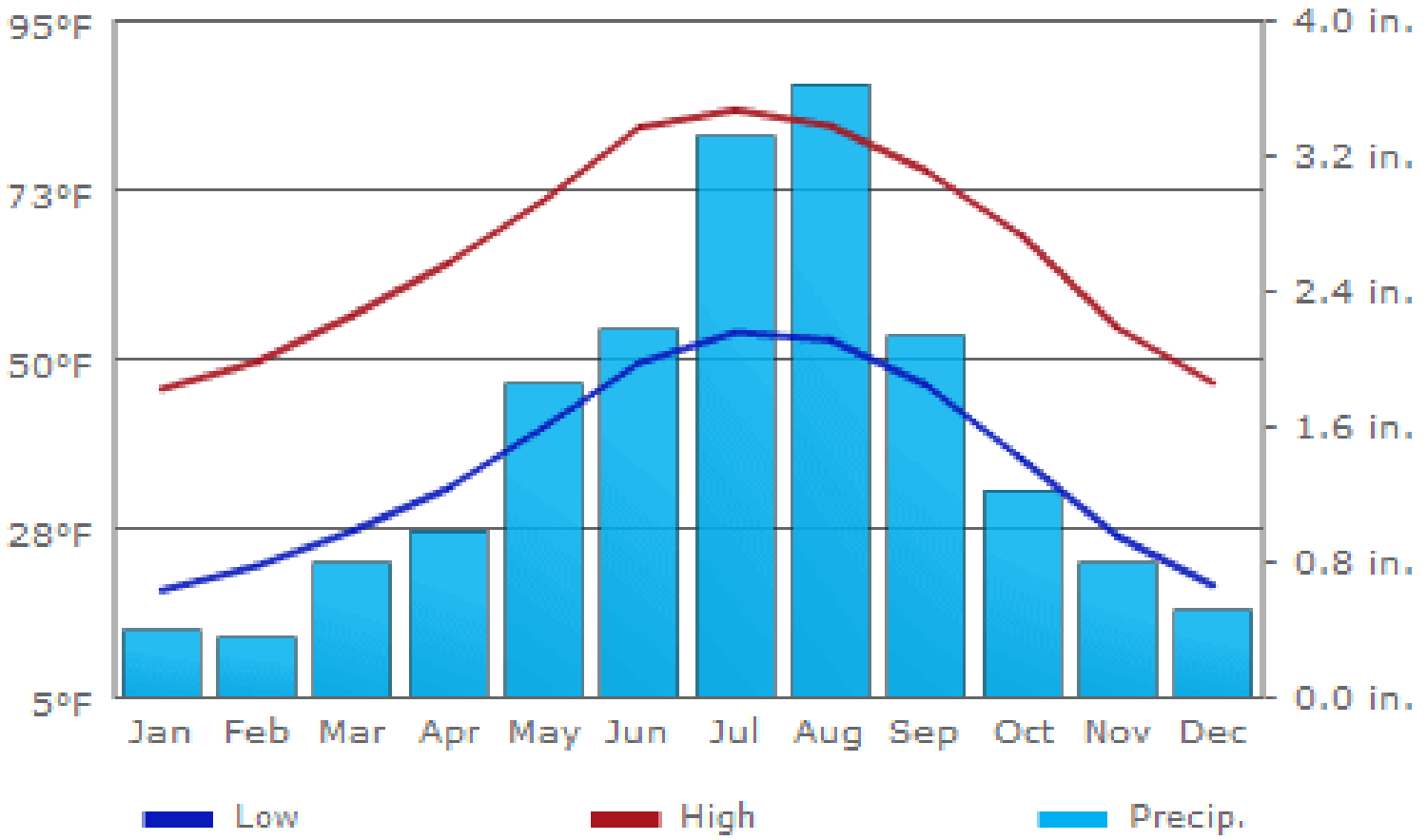

Figure 17: US-city-data.com graph of Las Vegas, NM annual monthly precipitation with average high and low temperatures.

1.4.4.2.2 Surface Water

An ephemeral stream that is fed by precipitation runoff drains most of the area of Ojitos Frios, including the three ranches that contain the well fields of this study. This stream, the Agua Zarca, runs east to west and discharges into the Gallinas River after cutting through the hogbacks and flowing down into the Las Vegas Plateau (Figure 10).

Just north of Ojitos Frios is the Gallinas River, a tributary to the Pecos River, which runs into the Rio Grande River (Figure 9). The watershed of the Gallinas encompasses ~84 sq. mi. (Evans and Lindline, 2004) and originates at 11,660 ft on the southeast slopes of Elk Mountain in the Sangre de Cristo Mountains (Aguirre, 2009). The melt from these snows in April to June and precipitation from July to September afford average daily flows of 15 cubic feet per second (cfs). However, flood and storm events may provide flows that exceed 250 or 500 cfs (Aguirre, 2009). Due to either natural recharge or irrigation returns, the river is classified as a gaining stream, but it also experiences many man-made diversions. The most pertinent diversion lies just north of the study area and adjacent to the Montezuma Hot Springs, located at what is classified as the Middle Gallinas Area. The diversion is called the United World College, and it supplies the Bradner and Peterson reservoirs (Aguirre, 2009). A major issue driving analysis of groundwaters in the Hogback area is the excessive diversion of surface water from the Gallinas (Figure 11).

1.4.4.2.3 Groundwater

While the city of Las Vegas is overdrawing from its surface water reservoirs (City of Las Vegas, 2010), it is not using the entirety of its 1,500 acre-foot water right (City of Las Vegas, 2010). One reason for this is that municipal and private wells in the developed city limits on the Las Vegas Plateau have low yields (New Mexico Office of the State Engineer, 2011). The Taylor Wells were drilled in the 1950s, but were only expected to be used for emergency drought use (Sundance Specialists Ltd. A). With increased demand, Taylor Well #4 is now continuously pumped, and the city is investigating development of the other wells in the area, specifically the

wells on the Milliken Ranch (Milliken, 2007). While these wells have a large output and are not as deep as the Taylor wells, they are further from the city, necessitating costly transportation into the city (Sundance Specialists Ltd. B). In addition, subdivision residents south of the ranches contest further municipal groundwater use on the grounds that continued pumping of wells up the flow gradient will adversely affect the quality and yield of residential groundwater wells (Milliken, 2007).

Groundwater in the area of Las Vegas falls into the OSE (Office of the State Engineer) declared Upper Pecos basin (Appendix D). The study area lies at the border of the mountains and the plateau, but still within the Sangre de Cristo Mountains. Wells throughout these mountains draw from the preCambrian (pC) metasedimentary rocks and the Sandia (not shown), Madera (not shown), Glorieta (Pg) and Sangre de Cristo (Psc) formations (Figure 18, City of Las Vegas, 2010). The majority of the wells sampled for this study tap the Sangre de Cristo formation; this is why the aquifer is referred to as the Sangre de Cristo in this paper. Like most of the formations in the area, the Sangre de Cristo relies on secondary permeability (Shomaker, 2007).

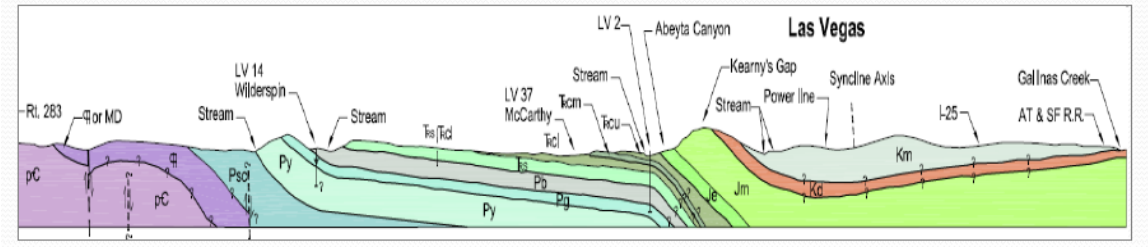

Figure 18: Las Vegas area local geology with formation ages and names marked. For more stratigraphic information see Appendix B.

1.4.4.2.4 Flow direction

According to a number of factors, the groundwater flow of the area is to the southeast. First, as mentioned above, all of the surface water in the region flows to the southeast in the form of rivers escaping the Rocky Mountain chain toward the Gulf of Mexico. This is true for the

Upper Pecos River watershed, which converges with the Rio Grande to flow southeasterly toward sea level (Figure 7). Second, an ancillary to the first, is the topography of the area and the elevation gradient that these features create. Moving both west to east and north to south, the elevation continuously decreases as the Sangre de Cristo Mountains transitions to the Las Vegas Plateau (Figure 10). Groundwater flow does not always follow topography, but depth to water measurements from drilling records of wells in the Las Vegas area show that the water table elevation continuously decreases in a southeasterly direction (Table 1). The short mention above of the highly permeable formations and the direction of dip in the area reinforces that groundwater has the ability to move with relative ease through the subsurface in the easterly direction of the geological inclination. Examining the series of cross sections at each Milliken well (Figure 15) shows that the dip of the formations decreases moving away from the Gallinas River. This indicates that infiltration from the river may be enhanced and as a possible water source.

Table 1: Change in Water Table Elevation

Location	Latitude	Longitude	Elevation (ft.)
Gallinas River in Mountains	35° 39' 05.39"	105° 18' 08.47"	6800
Devil's Gulch Well DTW	35° 36' 25"	105° 16' 34.1"	6381
Fork Well DTW	35° 35' 26.6"	105° 16' 33.4"	6369
Generator Well DTW	35° 32' 54.7"	105° 16' 05.5"	6259
Gallinas River on Plateau	35° 31' 34.37"	105° 12' 43.12"	6200

1.4.4.2.5 Breccia Zone

With this southeasterly flow and the amount of water infiltrating the exposed metasedimentary rock west of the hogback region, one would expect a high amount of groundwater in this final reach of the mountain block. However, in the description of the Montezuma Hot Springs, Bejnar and Bejnar (1979) describes the breccia zone at the Peterson Reservoir as a low permeability dam that hinders eastward moving groundwater. This breccia

feature is projected to extend 8 miles North-South, which means that groundwater encountering the zone along its length should be subject to flow impediment. It is indeed the case that the majority of wells east of this zone exhibit low yield, but the wells on the Taylor and Milliken ranches tested in this study yield from 200-900 gallons per minute (gpm) (Glorieta GeoScience, 1996). The difference between these wells and the others is that the former reach depths exceeding 600 ft (Shomaker, 2007). Figure 16 shows the projected vertical extent of the breccia zone is 2000 ft. If this low permeability feature is acting as a barricade against shallow, local flow, groundwater wells on the ranches to the east may be supplied by waters coming from a deeper, regional flow that passes beneath the breccia zone (Figure 16).

1.4.5 Flow Regimes

1.4.5.1 Regional

Regional flow for the study area would begin at Southern Rocky Mountaintops north of the Sangre de Cristo subrange. The water would percolate deep to create a regional flow regime traveling southeast through basement rock. Although the Sangre de Cristo aquifer is high in the stratigraphic column, deep, regional flow can be a significant recharge source (Wahi et al., 2008). In tectonic and fault zone areas, specifically, aquifers can receive regional groundwater through fractures and faults that act as upward conduits. While faults can also act as a barrier to retard flow, behavior in faults that facilitate flow is mainly controlled by the relative percentage of fault structures, fracture permeability and grain scale permeability (Apaydin, 2010). In the case of the breccia zone, the damage zone impedes water movement, due to the weak, incompetent nature of the rock. The Glorieta fault core is a water conduit, however, because recent faults and faults created by compression tend to be open (Wahi et al., 2008). Subsequent faults in the same area, thus, are likely to be open because they are formed by the same compressional forces. These fault zones have parallel sets of joints and fractures that increase the secondary permeability of the aquifer considerably (Apaydin, 2010). The area is also a syncline, a structural element that is also conducive to flow parallel to its axis (Apaydin,

2010). There is a large possibility that the deeply penetrating faults shown on Figure 16 may be acting as conduits for water from a deep, regional flow source.

1.4.5.2 Local

Aside from regional flow, the second possibility for an aquifer recharge source is local flow (Freeze and Cherry, 1979). While regional flow recharge would be accomplished by upward movement through permeable fault zones (Folch et al., 2008), local flow recharge would occur from local water sources, including both infiltration from local precipitation through the surface and from melt water surface bodies like the Gallinas and its reservoirs (Chowdhury et al., 2008). This infiltrated water flows easterly/southeasterly toward the Gallinas River in the Las Vegas basin. In order for local flow to recharge the Sangre de Cristo, it must past through or under the breccia zone.

1.5 Hypothesis

The two possible flow regimes replenishing the Sangre de Cristo aquifer are either local or regional. As flow has been identified as southeasterly, the implication of a regional flow regime entails similar characteristics between groundwater ascending into the aquifer and water from higher elevations to the northwest. As is evident in Figures 1 and 2, water from north of the area maintains a more negative stable isotopic value than local precipitation. Local flow, however, would maintain a stable isotope composition that reflects infiltration from local water sources fed by local precipitation. The contention of this work is that source conclusions will favor local flow with the possibility of mixing.

CHAPTER 2

METHOD

2.1 Sampling

A total of three trips to the Las Vegas, NM area were taken for field work at the study area. The first was made in the summer of 2009 for structural and stratigraphic mapping of the area. The second was in September 2009 and the third was in May 2010, both for the purpose of surface and ground water sampling.

2.1.1. Groundwater Sampling

Six wells total were sampled, five on the Milliken Ranch and one on the Taylor Ranch (Figure 18). The wells sampled follow a southeasterly trajectory away from the Gallinas River and were all sampled according to guidelines from the North America Quality of Water Assessment (NAQWA) field manual (NAQWA, 1995). Contact was made with the ranch owner, who provided a field hand, truck and a generator to be transported from well to well. The generator provided the power to the pump and each well was purged of three times its volume. After purging, ground water was pumped into a sterilized cooler to measure pump rate and to take physical parameters. Samples were taken from the cooler in the following order: a 1000 mL Teflon bottle raw sample, a 125 mL Teflon bottle for dissolved ions, a 125 mL Teflon bottle for total ions. The third bottle was treated with HNO_3 in the field. The bottles were immediately capped, labeled and stored in an iced cooler. The ice in the cooler was refreshed and double packed for shipping back to the UTA lab. The samples arrived at the lab with ~75% ice content, and the bottles were introduced to a refrigerator for storage until analysis. The following table includes pertinent information about each well.

Table 2: Groundwater Sample Location Information

Site - ID	Name	NMOSE#	Perforation Interval (ft.)	Depth to Water (ft.)	Formation	Date
A – ITW	Top	UP-3876	378 - 630	200.05	Pp	9/2009
B – IDGW	Devil's Gulch	UP-3874	706 - 790	478.52	Sc	5/2010
C – IFW	Fork	UP-3873	590 - 690	370.79	Sc	9/2009
D – IMB	New Barn	UP-4174	500 - 600	345	Sc	5/2010
E – ITMW	Taylor 4	UP-12452	50 - 826	50	All	5/2010
F – IGW	Generator	UP-3374	540 - 600	341	Sc	9/2009

NMOSE – New Mexico Office of the State Engineer

2.1.2 Surface Water Sampling

Five surface water samples were collected at points on or near the Gallinas River and two at points on the Milliken Ranch (Figure 19). The surface water sampled was taken in accordance to the guidelines from the Hem's USGS water-supply paper (Hem, 1985). Points in the water feature with minimum clouding and maximum flow were visually picked and the three Teflon bottles were filled with the mouth pointing in the flow direction. The samples were taken in the following order: a 1000 mL Teflon bottle raw sample, a 125 mL Teflon bottle for dissolved ions, a 125 mL Teflon bottle for total ions. The third bottle was treated with HNO_3 in the field. The bottles were immediately capped, labeled and stored in an iced cooler. The ice in the cooler was refreshed and double packed for shipping back to the UTA lab. The samples arrived at the lab with ~75% ice content, and the bottles were introduced to a refrigerator for storage until analysis.

Table 3: Surface Water Location Information

Site – ID	Location	Date	Comment
G – IGR	Gallinas River	Sep-09	From thalweg
H – IGRII	Gallinas River	May-10	From thalweg
I – IMB	Montezuma Hot Springs	Sep-09	Standing hot spring pool
J – IPR	Peterson Reservoir tributary	May-10	Moving channel into reservoir
K – IBR	Bradner Reservoir	May-10	Standing water body
L – IDGP	Devil's Gulch Pond	Sep-09	Standing water body
M – IDGR	Devil's Gulch Stream	Sep-09	Ephemeral, snowmelt stream

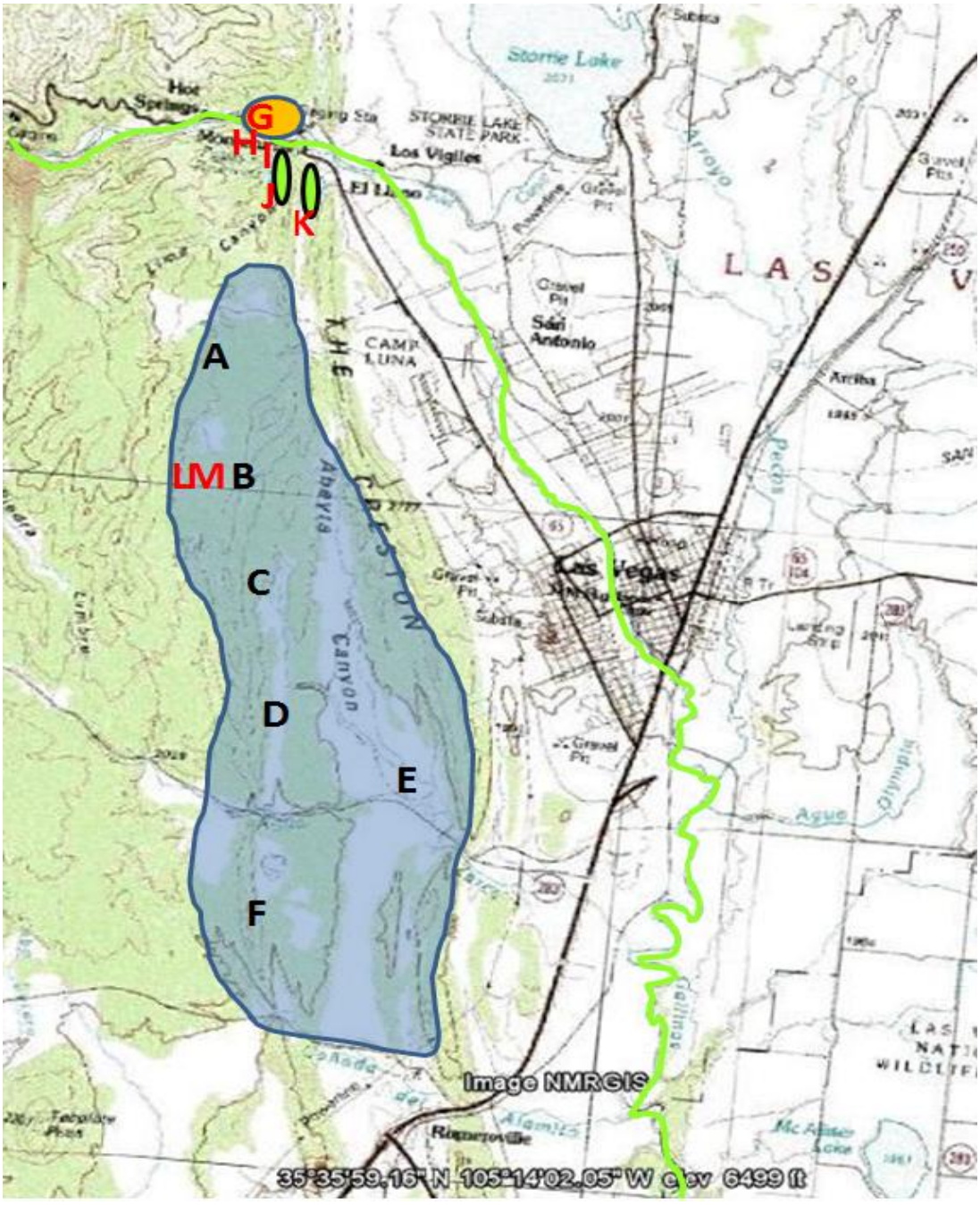

Figure 19: Georeferenced USGS quadrangle topographic map of thesis area with sampling points marked as letters from Tables 2 and 3.

2.2 Analysis

Upon arrival at the lab, the samples underwent treatment that is generally carried out in the field, but was done later due to equipment constraints. This treatment included measurement for TDS, pH and temperature (Appendix E). In addition, the samples were filtered using a Brand vacuum pump and Supor .45 µm filter paper. From each 500 mL bottle, 200 mL was filtered and stored in a new 200 mL Teflon bottle. The first 125 mL bottle was filtered, and then treated with 0.1% HNO_3 to observe any potential colloidal in the elements. The second 125 mL bottle was also filtered. These three bottles were then ready for analysis. The remaining 300 mL was kept in the 500 mL bottle as a raw sample.

2.2.1 Stable Isotope Analysis

2 mL from every filtered, non-acidified sample was aliquoted into a rubber stopped, 3 mL glass bottle and sent in padded packaging to Texas State University for analysis by Dr. Benjamin Schwartz. The samples were run on August 24, 2010; the following is his description of the steps taken:

"The instrument used is a Model 908-0008, Los Gatos Research (LGR), Liquid Water Stable Isotope Analyzer. This instrument uses Off-Axis Integrated Cavity Output Spectroscopy (OA-ICOS) laser technology to simultaneously measure Hydrogen and Oxygen stable isotopic ratios from liquid water samples. All data found in the attached sheet are reported relative to VSMOW. Samples are prepared in 2 mL glass vials that are loaded into an autosampler attached to the instrument. Each sample is analyzed 8 times and the first 2 analyses are ignored to eliminate the effects of 'sample memory.' Measurement accuracies are generally better than ±0.4‰ for δD and ±0.1‰ $\delta^{18}O$. However, a sample standard deviation is reported for each sample. Compounds that may affect the accuracy of the analysis include, but are not limited to: organic compounds and salts. For highly saline or mineralized waters, we distill the water prior to analysis. Distillation involves taking a ~2 mL split of the sample and completely distilling it using an apparatus designed for extracting plant-water samples for isotopic analysis.

During each batch run, internal standards are run at the beginning and end of each run, and after every third unknown sample, to allow for correction of potential instrument drift. Internal standards were created using Certified Standards obtained from LGR, and have been verified by an external lab. In addition, each run includes a standard which is analyzed and processed as an unknown. Raw data are post-processed in a LIMS system developed and customized for LGR data by Tyler Coplen at the USGS, Reston."

2.2.2 Elemental Analysis

The acidified samples from the two 125 mL Teflon bottles were analyzed for major, minor and trace elements using the quadrupole inductively coupled plasma-mass spectrometry system (ICP-MS) at the University of Texas at Arlington's Hydrogeochemistry lab.

All the aqueous samples were prepared in 1% high-purity nitric acid (Arista Ultra, VWR, Radnor, PA). A rinse solution of 1% high-purity nitric acid was also used between samples to remove potential memory effects. A solution containing four internal standards (Li-6, Sc-45, In-115, and Bi-209) at 10 µg/mL was introduced to each sample to provide a basis for time-drift correction and to monitor potential signal response changes from the ICP-MS. For each sample, signal response (in counts per second, cps) for each element was then normalized with the signal response of the standard with the most similar mass. The mass-dependent normalizations revealed that these 4 internal standards followed a similar trend throughout the duration of the sample analyses. This allowed the designation of only In-115 as the internal standard for drift correction.

The major elements (K, Na, Ca, Mg, and Si) were measured with a sample dilution factor of 50, with 0.1 mL sample and 4.9 mL 1% high-purity nitric acid. A standard series of these multiple elements were prepared at the concentration of 0, 1, 4, 20, 100, 400, and 2000 µg/L to obtain the calibration curves. Furthermore, a standard solution with 100 µg/L major elements was periodically measured, the same way as a sample, for every 10 samples to check the validity of analyses.

A total of 58 minor and trace elements (e.g., Al, Fe, Mn, Rb, Sr, Mo, Th, and U) was analyzed with 4.95 mL sample spiked with 0.05 mL concentrated nitric acid (to achieve the same matrix of 1% nitric acid, as the standards). The standard series of 0, 0.1, 0.5, 2, 10, 40, 200, and 500 µg/L for the 58 elements were prepared to generate the calibration curve. A standard solution with 100 µg/L minor and trace elements was periodically measured after every 10 samples to check the validity of analyses.

2.2.3 Carbon and Ion Analysis

2.2.3.1 TOC

The TOC (total organic carbon) concentration of the water samples was quantified by measuring the non-purgeable organic carbon (NPOC) concentration, using a TOC analyzer (TOC-VCSH/CSN, Shimadzu) with a furnace temperature at 680 ^{o}C, acid ratio of 1.5% and a purge time of 1.5 min. Duplicate measurements of TOC were made. A TC (total carbon) standard series of 0, 1, 2, 3, 4 and 5 mg/L concentration was made from 1000 mg/L stock solution, prepared with reagent grade potassium hydrogen phthalate previously dried at 105 ^{o}C for an hour and cooled in a desiccator, and the area signal obtained to quantify the sample concentration.

2.2.3.2 IC

IC (inorganic carbon) standard series of 0, 1, 2, 3, 4 and 5 mg/L concentration was similarly made from 1000 mg/L stock solution, prepared with reagent grade sodium hydrogen carbonate previously dried in a desiccator for 2 hours and sodium carbonate previously dried at 280 ^{o}C for an hour and cooled in a desiccator. Another solution was prepared by diluting 50 mL of 85 % reagent grade phosphoric acid to a final volume of 250 mL for IC analysis.

2.2.3.3 Ions

A Dionex (Dionex Corp., Sunnyvale, CA) ion chromatography DX-500 system was used in this study to analyze common anions (F^-, Br^-, Cl^-, NO_2^-, NO_3^-, SO_4^{2-}, and PO_4^{3-}). The system consisted of a GP50 pump, a conductivity detector CD25A with a thermal compartment for

temperature control, and an anion self-regenerating suppressor (ASRS) that operated at 50 mA in the recycled-water mode. An IonPac AS14 (4 × 250 mm; 4-mm inner diameter and 250-mm length) analytical column was used to separate all anions. An IonPac AG14 (4 × 50 mm; 4-mm inner diameter and 50-mm length) guard column was placed prior to the analytical column to prevent potential fouling of the analytical column. Both analytical and guard columns were maintained at 35 °C for signal stability. With the eluent of 3.5 mM Na_2CO_3 and 1.0 mM $NaHCO_3$, at the flow rate of 1.0 mL/min, all of these seven anions can be separated and quantified in less than 12 min. An injection loop size of 25 µL was used for sample analyses, with an automated sampler (AS 40). Finally, data manipulation and the operation of all the components in the system were controlled by Chromeleon version 6.80, Dionex chromatographic software.

The standard series of 0, 0.01, 0.04, 0.1, 0.4, 2, and 20 mg/L for all seven anions were prepared to generate the calibration curve. A standard solution with 1 mg/L of these 7 anions was periodically measured after every 10 samples to check the validity of analyses.

CHAPTER 3

RESULTS

3.1 Isotopic Results

The stable isotope values of the groundwater and surface water of the thesis area are shown on Table 3.1. The first set of values is of the groundwater samples, and they range from -50‰ to -75‰ and -6‰ to -11‰ for δD and $\delta^{18}O$ respectively. The second set is of the surface water samples, and they range from -42‰ to -98‰ and -2‰ to -13‰ for δD and $\delta^{18}O$ respectively. Figure 3.1 shows the values plotted against each other, δD on the Y axis and $\delta^{18}O$ on the X axis, and in relation to the GMWL (global meteoric water line).

Table 4: Isotope Value Comparisons

	Bowen (2007) Precipitation Map	Yapp (1986) Precipitation	Lambert (1997) Mtn Precipitation	Study Samples
$\delta^{18}O$	-11.2 to 12.4‰	Not Available	>-12.1‰	-7.9 to -12
$\delta^{2}H$	-82 to -92‰	~-60‰	>-86‰	-58 to -79‰

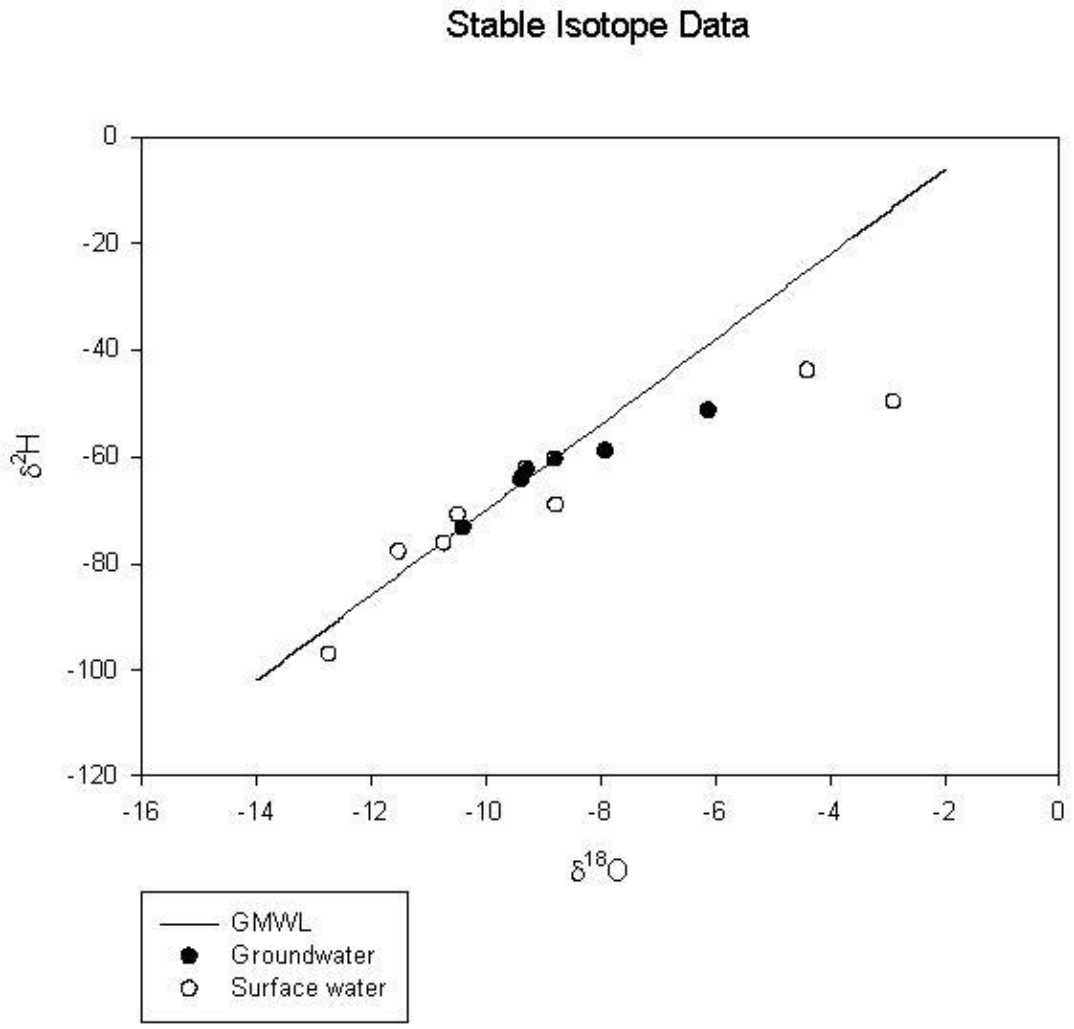

Figure 20: Stable isotope data plot for surface and groundwater.

In general, the groundwater samples are more positive than the surface water samples with the exception of the surface water samples taken at standing pools, the Bradner reservoir and the Devil's Gulch Pond, which veer from the other surface samples and from the GMWL due to evaporation effects. Another anomaly in the surface water data is the Devil's Gulch Ravine data, which is much more negative than the other samples. More negative values are associated with snow melt, and this sample was taken from the snow melt water of the slowly

flowing stream running atop the ravine between the Devil's Gulch Pond and the Devil's Gulch Well. Some variation is also expected due to seasonal variability.

3.2 Chemical Results

3.2.1 Piper Plot

The ionic concentrations of the water samples in mg/L were plotted on the Piper plot shown on Figure 21. Aside from the Hot Springs sample and the Taylor Well sample in the Ca-Mg-SO_4-Cl group, all of the samples plot in the Ca-Mg-HCO_3 group.

3.2.2 Ion Plots

The values of the ion analysis are shown as ion plots on the left column of Figures # 22-30; the chemical results of Shomaker (2007) are presented for comparison on the right column of Figures # 22-29. The plot and their results are summarized below on Table 5.

Table 5: Ion Plot Trends

X vs. Y	Trend - Study	Trend - Shomaker
Cl^- vs. Mg^{2+}	None	Linear moving South
Na^+ vs. SO_4^{2-}	↑SO_4^{2-} moving South	Linear moving South
Na^+ vs. Cl^-	None	Linear moving South
Ca^{2+} vs. Na^+	Cluster	↑Na^+ moving South
Cl^- vs. Ca^{2+}	None	↑Cl^- moving South
Cl^- vs. SO_4^{2-}	None	↑Cl^- moving South
Ca^{2+} vs. Sr^{2+}	↑Sr^{2+} moving South	↑Sr^{2+} moving South
Ca^{2+} vs. SO_4^{2-}	None	Cluster
Cl^-/Br^- vs. Cl^-	Linear, Non-spatial pattern	Not Available

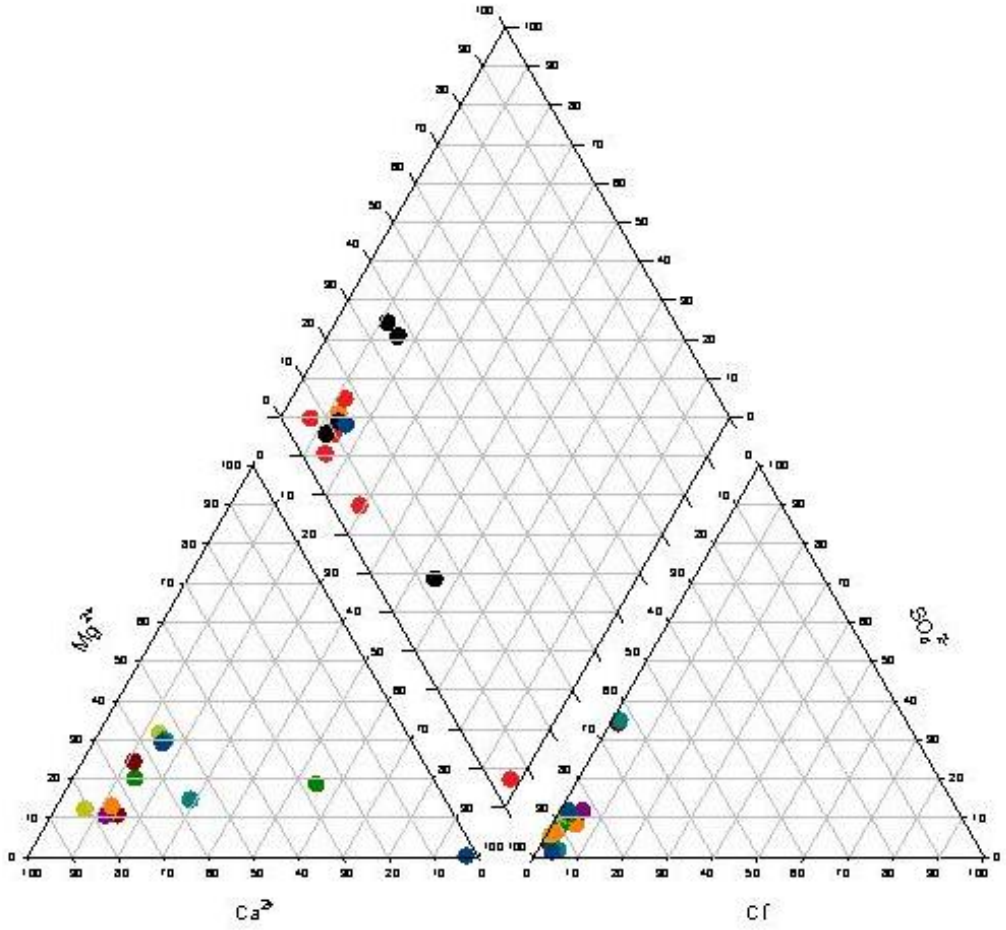

Figure 21: Piper diagram for chemical grouping. Groundwater and surface water values are designated on the diamond plot. Groundwater is represented by dark colors (black and midnight blue). Surface water is represented by bright colors (red and orange).

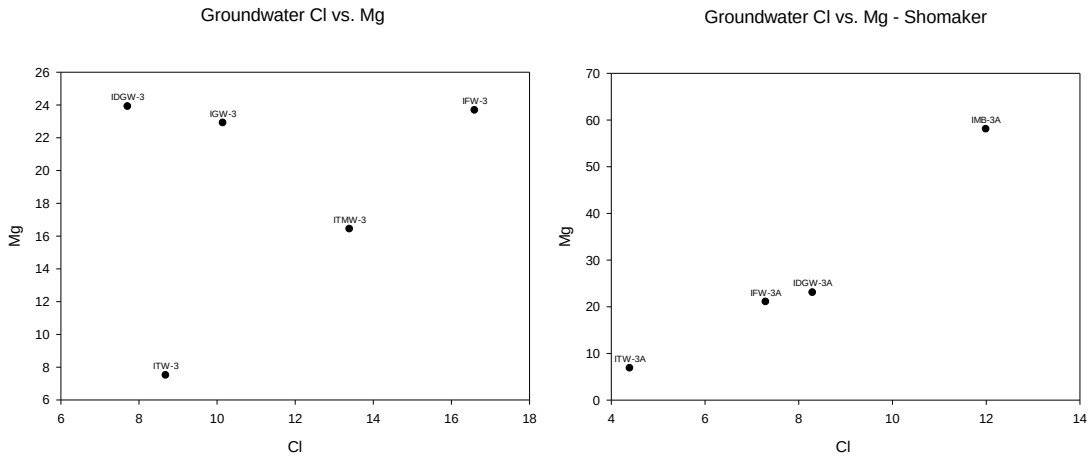

Figure 22: Ion plot of Cl^- vs. Mg^{2+} with Local ID labels to assess change with distance from the river.

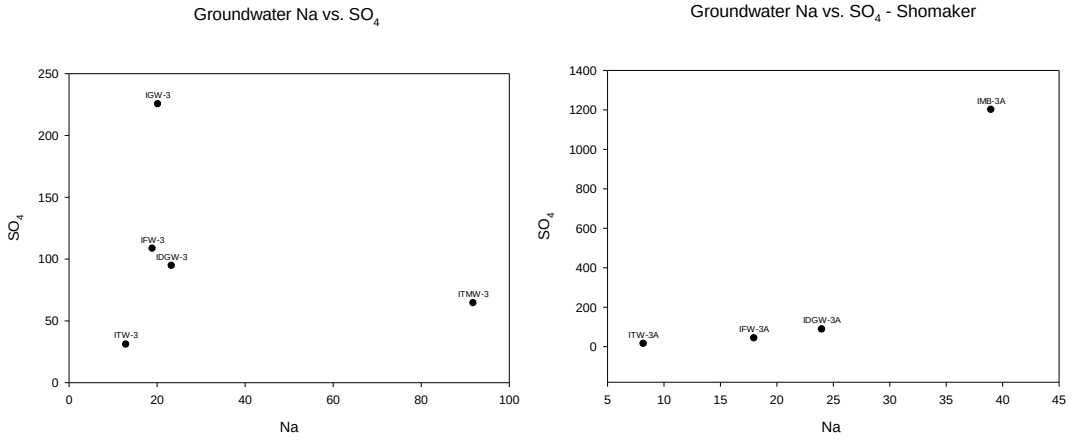

Figure 23: Ion plot of Na^+ vs. SO_4^{2-} with Local ID labels to assess change with distance from the river.

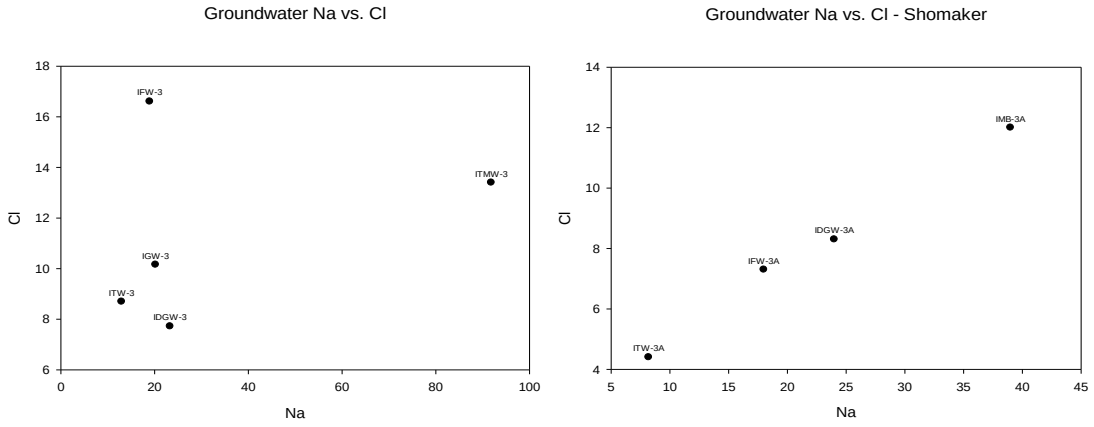

Figure 24: Ion plot of Na^+ vs. Cl^- with Local ID labels to assess change with distance from the river.

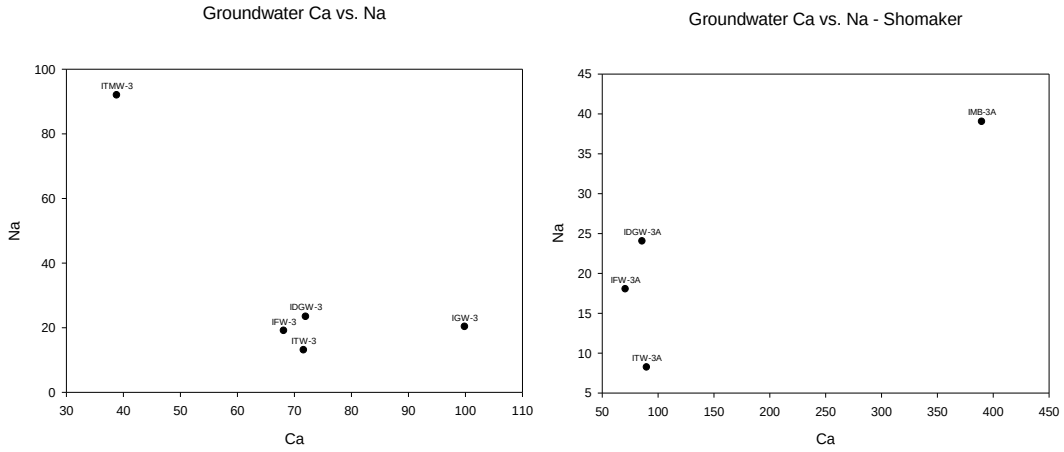

Figure 25: Ion plot of Ca^{2+} vs. Na^{+} with Local ID labels to assess change with distance from the river.

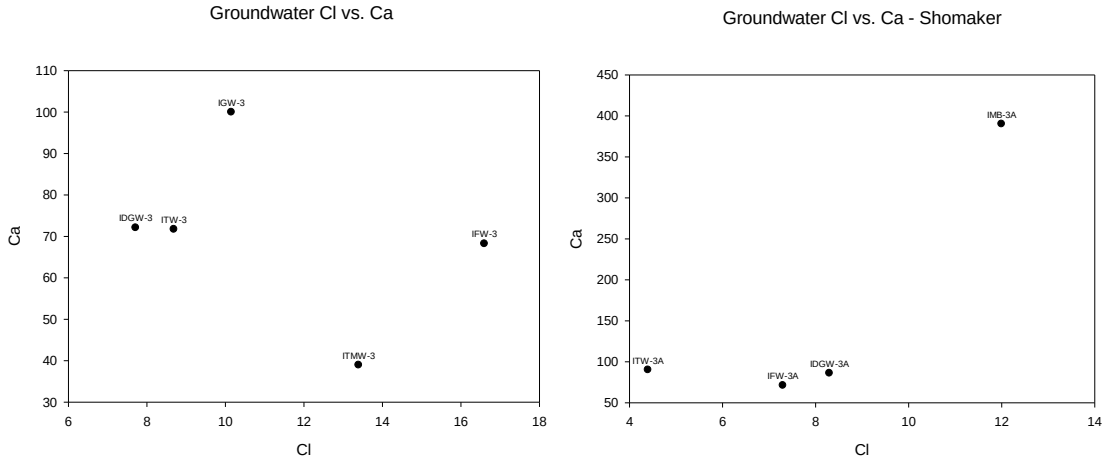

Figure 26: Ion plot of Cl^{-} vs. Ca^{2+} with Local ID labels to assess change with distance from the river.

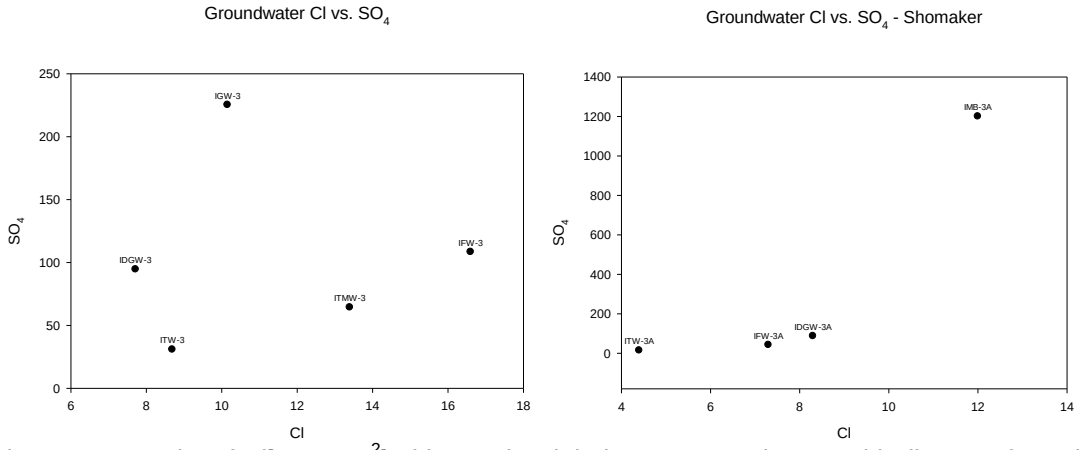

Figure 27: Ion plot of Cl^{-} vs. SO_4^{2-} with Local ID labels to assess change with distance from the river.

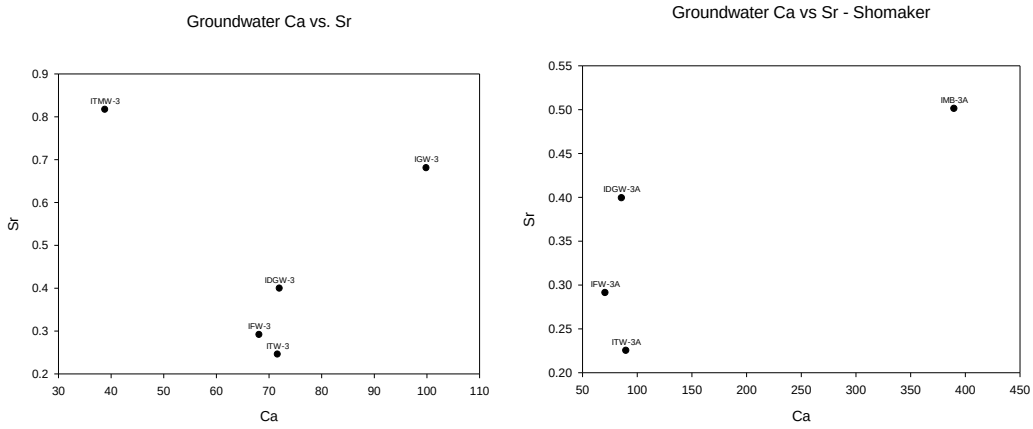

Figure 28: Ion plot of Ca^{2+} vs. Sr^{2+} with Local ID labels to assess change with distance from the river.

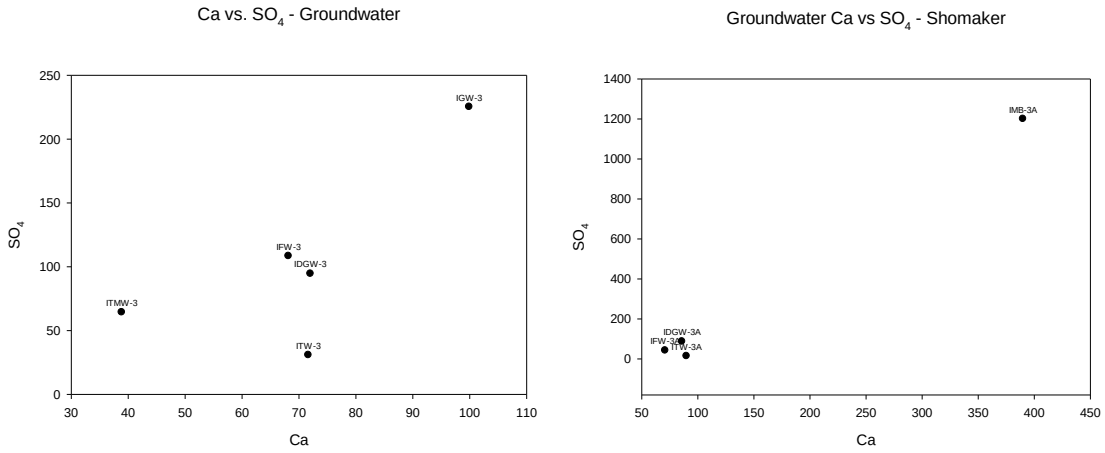

Figure 29: Ion plot of Ca^{2+} vs. SO_4^{2-} with Local ID labels to assess change with distance from the river.

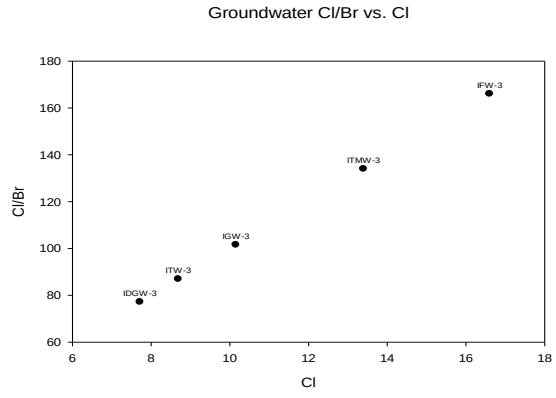

Figure 30: Ion plot of Cl^-/Br^- vs. Cl^- with Local ID labels to assess change with distance from the river.

CHAPTER 4

DISCUSSION

4.1 Stable Isotope Data

This study used hydrogeochemical testing of water samples in order to correlate surface water associated with local flow sources to deep well groundwater in the Sangre de Cristo aquifer. The pivotal pair of parameters for making this correlation is the stable isotope ratios of oxygen-18 to oxygen-16 and deuterium to hydrogen.

4.1.1 Results vs. Interpolated Map

Figure 20 shows a plot of δ^2H vs $\delta^{18}O$ for all the waters tested in this study. The surface water is represented by dark circles and the groundwater is represented by light circles. The majority of the samples plot on or near the GMWL, which means that the sample water has recently been part of the water cycle in the form of precipitation (White et al., 1973). An obvious cluster along the GMWL contains both dark and light circles. The proximity of the values hints that the waters in the cluster come from a similar source. As the water is meteoric in origin, the value range can be compared to the IAEA precipitation maps on Figures 3 and 4 to ascertain the geographic origin of the rain (Bowen et al., 2007). The area of Las Vegas, denoted as a black dot, lies on the aqua blue band on both maps. The hypothetical range of values for the Las Vegas area, then, is from -82 to -92 and -11.2 to -12.4 for δ^2H and $\delta^{18}O$ respectively. The experimental ranges of the points on Figure 20's cluster range from -58.88 to -77.79 for δ^2H and -7.92 to -11.52 for $\delta^{18}O$. According to these maps, none of the δ^2H and only some of the $\delta^{18}O$ experimental values fall within the hypothetical range for precipitation falling in the area of Las Vegas.

As the stable isotope values from the Hogback area do not match the map's interpolated value for the area around Las Vegas, precipitation falling on the areas that do

match the colors corresponding to the experimental values may be the source of said water. These ranges encompass multiple bands on both maps: yellow (-53 to -62), yellow-green (-63 to -71) and sea green (-72 to -81) on the δ^2H map and the yellow-green (-8.8 to -9.9), sea green (-10 to -11.1) and aqua blue (-11.2 to -12.4) bands on the $\delta^{18}O$ map. All of these color bands appear southeast of the black dot denoting the area around Las Vegas. However, flow for both surface and groundwater is oriented to the southeast (background – hydrology – flow direction). Recharge occurs in uplands (Freeze and Cherry, 1979), so recharge from precipitation falling into the areas colored yellow, yellow-green or sea green is not possible.

Since the maps are interpolated based on geographically disparate data points, they should not be considered an unquestionable resource for all precipitation data. In addition, the study of Yapp's (1986) Albuquerque data records how precipitation values in this adjacent area vary temporally. These variations are due to factors like the initial moisture source of the rain producing air masses and the type of precipitation sampled. Yapp (1986) records a precipitation δ^2H range from -6 to -158 with an average δ^2H value of ~-60. This average value differs from the range presented by the interpolated, color coded map, but falls within the range of the cluster from Figure 20. Using this value as the indicator for meteoric water in the region places the Las Vegas data in the range for recharge by local, meteoric water.

4.1.2 Local vs. Regional

While the interpolated δ^2H and $\delta^{18}O$ maps are not definitive identifiers of precipitation stable isotope values in a region, they are useful because the pattern of color bands indicates the continental effect for precipitation over the Southwest. As rain producing clouds move inland from their Pacific Ocean moisture source, the heavier isotopes preferentially rain out and the stable isotope value of precipitation becomes increasingly light moving inland. This pattern demonstrates that isotope values that are heavier (more negative) are sourced from precipitation falling closer to the west coast.

Precipitation falling on peaks of the Southern Rocky Mountains up the flow path, that is, to the north and northwest, have a heavier isotopic value than precipitation falling on the local study area. These peaks are the probable recharge zones of a deep flow regime, so if groundwater stable isotope values in the Hogback area are more negative than the local value for meteoric water, then the wells are tapping regional flow. Whether the value accepted for the local, meteoric recharge comes from the interpolated map, from the sampled surface water or from the study done by Yapp (1986), the groundwater values are not significantly more negative. Therefore, the groundwater from the Hogback area does not emanate from a deep, regional flow regime that is recharged by distant precipitation on mountaintops to the northwest.

The two options for recharge presented were from regional and local flow regimes. The groundwater values were not negative enough with respect to the local precipitation value to definitively point to a regional flow pattern, so the other possibility, local flow, must be examined. Local flow is recharged by infiltration from local precipitation and from mountain streams fed by snow melt and runoff. Its viability as a recharge source can be examined with stable isotopes by comparing the values of groundwater and surface channel water stable isotope values. If the values are similar, the possibility of local flow recharge is high.

Testing surface water channels for stable isotope values can be problematic due to the effects of evaporation and the variability of rainwater input quantities during different times of year. Input from melt water and runoff from precipitation may also vary the values of channel water. All of these issues may have made an impact on the values taken for the Gallinas River. This was evident for the sample from the Peterson Reservoir, for instance, which shows a considerable evaporative deviation from the GMWL. The two samples taken at the same point on the river during fall and spring fall very near one another, but one does veer slightly off the GMWL. As Figure 9 shows, however, the Gallinas River is sourced from the top of nearby Elk Mountain, so only such slight variations are expected. Even with these variations, the cluster of points on the GMWL of Figure 20 clearly shows that samples taken at the river and at its

diversions are similar to the values of the sampled groundwater. This similarity points to local flow as the main mechanism of groundwater recharge.

4.1.3 Change with Distance

Looking at the cluster of the δ^2H vs. δ^{18}O graph, more of the light circles are on the left side of the group and the dark circles tend to favor the right side. While considerable overlap occurs, a division between the two groups is apparent around -10.5 and -75, separating lighter groundwater values from heavier surface water values. This disparity shows that the flow regime must be local since groundwater from a regional flow regime would come from more negative precipitation falling on mountain areas to the northwest of the study area.

This division may provide more information about the recharge mechanism if examined for change with distance from the river. An observable pattern of change with distance would further validate recharge from local precipitation, specifically from surface channel infiltration. Moving south from the area where the Gallinas River was sampled (Figure 19), the Milliken wells follow a southeasterly trajectory in the following order: ITW, IDGW, IFW, IMB, IGW. Looking at the graph (Figure 20), this order should be maintained moving away from the surface water points. The order is not maintained, but the possibility of infiltration from the Gallinas is still valid because the order is maintained if IFW is not included in the data set. An examination of chemical trends with distance is discussed further below.

4.2 Chemical Data

4.2.1 Piper Plot

According to the plot, most of the water samples belong to the Ca-HCO_3-Mg type of water. All of the surface water should be coming from precipitation in the local area, and the fact that local ponds and the Gallinas River belong to the same chemical group ascertains that the two belong to the same precipitation source. The wells belonging to this group may indicate a similar precipitation source, or may back up the hypothesis that surface water bodies are

leaking into the groundwater aquifer at a significant rate. The only surface water sample that did not plot in this group was the hot spring sample; it plotted in the SO_4-Cl-Ca-Mg group.

This hot spring sample, while taken at the surface, is sourced from groundwater that quickly moves to the surface. Compared to the other samples, the anion concentrations are similar, but the cations are very different, the largest discerning factor being the high Mg and K content. Given that the stable isotope data found that the hot springs water comes from a related, local flow regime, explaining the change in chemistry as a function of depth is probably inaccurate. Unlike water extracted from wells, the hot springs water passes through soil and bog to reach the sampled pools. Reaction with minerals in the soil like magnesite and mica is the most probable reason for this chemical deviation.

All of the groundwater plots lie within the chemical zone that the surface water belongs to, which vindicates the hypothesis that these waters belong to a similar flow regime. There is an obvious cluster within the group, however, but three of the wells fall outside of it. Chemically, the dissimilar factors of two of the outside wells are higher concentrations of HCO_3^- and Cl^-; the cation concentrations plot very near those of the other water samples. These first two wells differ from the others in that they lie in direct proximity to a surface water pond and an ephemeral stream. These surface water bodies are possibly contributing to this chemical increase by mixing with ground water. These surface waters may have high HCO_3^- and Cl^- from animal or pesticide inputs.

The third well that plots away from the main cluster of samples on the Piper plot is the Taylor Well, which plots with the hot springs in the SO_4-Cl-Ca-Mg group. This is the deepest of all the groundwater wells, and only slightly misses plotting in the Ca-HCO_3-Mg group. Located on the Taylor Ranch instead of the Milliken Ranch, it is situated much further to the East, near the Dakota Sandstone Hogback. Its distance and depth mean that there is more time for water-rock interactions that cause mineralization.

4.2.2 Ion Plots

Looking at the plots of this study's samples, the points are scattered randomly. While some point groupings are noticeable on a couple plots, only one, Na^+ vs. SO_4^{2-}, has a linear relationship that changes following the order of distance from the river. However, the chemical data from Shomaker's work in 2007 demonstrates several graphs with linear relationships as described above. Those that do not have linear relationships demonstrate parabolic ones with the closest and most distant wells maintaining their positions throughout. The relationships demonstrated by graphs made from Shomaker's data both call into question the reliability of this study's ion data and support the hypothesis of local recharge from the river channel.

4.3 Breccia Zone Implications

From the introduction, the extent and permeability of the breccia zone (Figure 16) underlying the Peterson Reservoir is as follows: 3 miles to the North, 5 miles to the South, 3000 ft. deep, 50 ft. wide and impermeable, acting as a dam for local flow moving east (Bejnar and Bejnar, 1979). As this study has shown, the interpretation of its water as a component of local flow is accurate. However, several wells on ranches to the east of this active dam experience very high yield water with isotopic signatures that link them to the same local flow regime supplying the hot springs (Shomaker, 2007). Local subsurface flow, then, is somehow bypassing this breccia zone to recharge the Sangre de Cristo aquifer.

This water may be passing underneath or through the whole breccia feature. The water may be accessing a fracture that cuts across the breccia zone, probably at the Devil's Gulch Ravine. The breccia feature may not be as long, as impermeable or as deep as previously accepted. As a topic of further study, the above characteristics of the breccia zone should be reevaluated and possibly revised.

CHAPTER 5

CONCLUSIONS

The goal of this research was to source the groundwater emanating from the wells on the Milliken Ranch in the Hogback area west of Las Vegas, NM. An assessment of the hydrology of the area from existing physiographic and hydrogeologic data indicated participation in a local southeasterly flow regime, while a study of a breccia feature of the Montezuma hot springs and the presence of deep faults and fractures suggested a source from a deeper, regional flow regime. Two season sampling was carried out in this study to correlate the deep groundwater of the ranches in the Hogback area to the upland surface water around the Gallinas River. From the analysis of the hydrogeochemical data of the samples, these conclusions have been reached:

- Water in the Hogback area comes from recent precipitation
- Wells in the Hogback area do not tap a regional flow regime
- The Sangre de Cristo aquifer is recharged by a local flow regime
- Surface water and groundwater belong to the same local flow regime with possible surface water leakage
- The breccia zone under the Peterson reservoir is permeable enough to allow flow to the Sangre de Cristo aquifer

Some suggestions for further investigations of hydrology in the Las Vegas and Milliken/Taylor Ranch areas are as follows:

- Take monthly precipitation samples to construct a Local Meteoric Water Line (LMWL)
- Take samples of shallow wells for comparison of change with depth and to confirm top down infiltration

- Sample surface water more frequently for a longer period of time
- Take parameters like temperature and pH into account (measured in field)
- Take water level measurements in area wells
- Sample wells north of the Gallinas River

APPENDIX A

ISOTOPE RATIO VARIABILITY

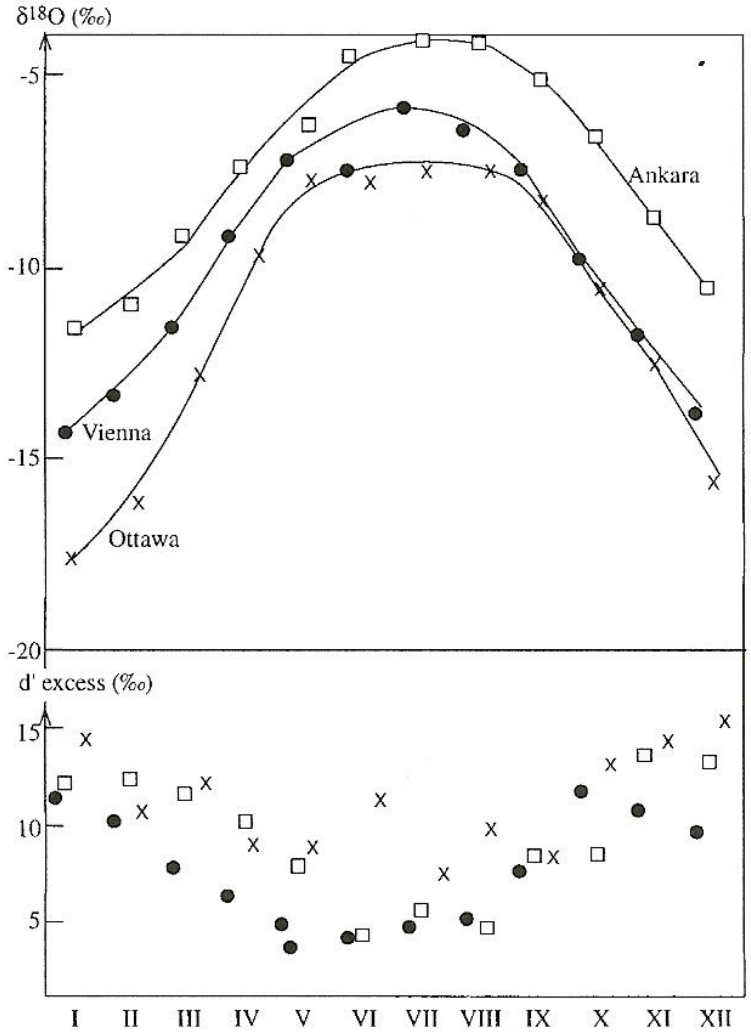

Figure 9 Seasonal change of $\delta(^{18}O)$ and d for selected continental stations, based on IAEA network data (IAEA 1992).

APPENDIX B

LAS VEGAS AREA STRATIGRAPHY

Stratigraphic Column Key

(Bejnar and Bejnar, 1979)

Period	Formation	Description	Thickness (ft)
Quaternary and Tertiary	Pediment and river gravels	Mixture of Precambrian and younger sedimentary rock clasts	40 max.
	Carlisle Shale (Kc)	Mostly dark-gray shale with sparse yellow-brown sandstone beds in upper half of formation	400
Cretaceous	Greenhorn Limestone (Kgh)	Alternating beds of medium-gray limestone with olive-gray shale	63
	Graneros Shale (Kg)	Medium-dark-gray shale with calcareous cement	225
	Dakota Sandstone (Kd)	Three units: Lower, pale-grayish-orange to very light gray sandstone, conglomeratic to fine grained, locally crossbedded. Middle, dark-gray carbonaceous shale. Upper, grayish-yellow to grayish-olive sandstone including coaly fragments	103
Jurassic	Morrison Formation (Jm)	Upper half, grayish-olive shale. Lower half, grayish-orange-pink, medium-grained sandstone alternating with thinner beds of siltstone and shale	415
	Todilto Limestone (Jot)	Medium-dark-gray, thin-bedded limestone interbedded with thin greenish-gray beds of siltstone and shale	20
	Ocate (Entrada) Sandstone (Jot)	Medium-grained grayish-yellow to pale-orange, flat to crossbedded, friable sandstone	127
Triassic	Chinle Formation (Trc)	Various shades of red siltstone ranging from medium red to grayish red, with alternating pale-olive to pale-red sandstones and conglomerates	1202
	Santa Rosa Formation (Trs)	Pale-reddish-brown to yellowish-gray sandstones and conglomerates interbedded with thinner layers of pale-olive to grayish-red shale	323
Permian	Bernal Formation (Pb)	Pale-reddish-brown, thin-bedded siltstone, shale, and sandstone interbedded	118
	San Andres Limestone (Pg)	Pale-yellowish-brown, dolomitic, dense limestone	6
	Glorieta Sandstone (Pg)	Grayish-orange, fine-to-medium-grained, bimodal, very resistant sandstone	93
	Yeso Formation (Py)	Faulted out in Gallinas Canyon	
Pennsylvanian	Sangre de Cristo Formation (PPsc)	Faulted out in Gallinas Canyon	
	Madera Formation (PPsm)	Dark-yellowish-brown to light-olive-gray, thin-bedded, fossiliferous limestone interbedded with pale-red to yellowish-orange thinner bedded shales	137
	Sandia Formation (PPsm)	Light-gray to dark-gray, fine-grained to coarsely crystalline limestone interbedded with pale-olive to dark-gray shale	172
Precambrian	Precambrian (pC)	Metasediments plus migmatites,	2,000+

APPENDIX C

LAS VEGAS EVAPOTRANSPIRATION

Figure B-6

Mora - San Miguel - Guadalupe Water Plan

Average Annual Free Water Surface Evaporation Rate

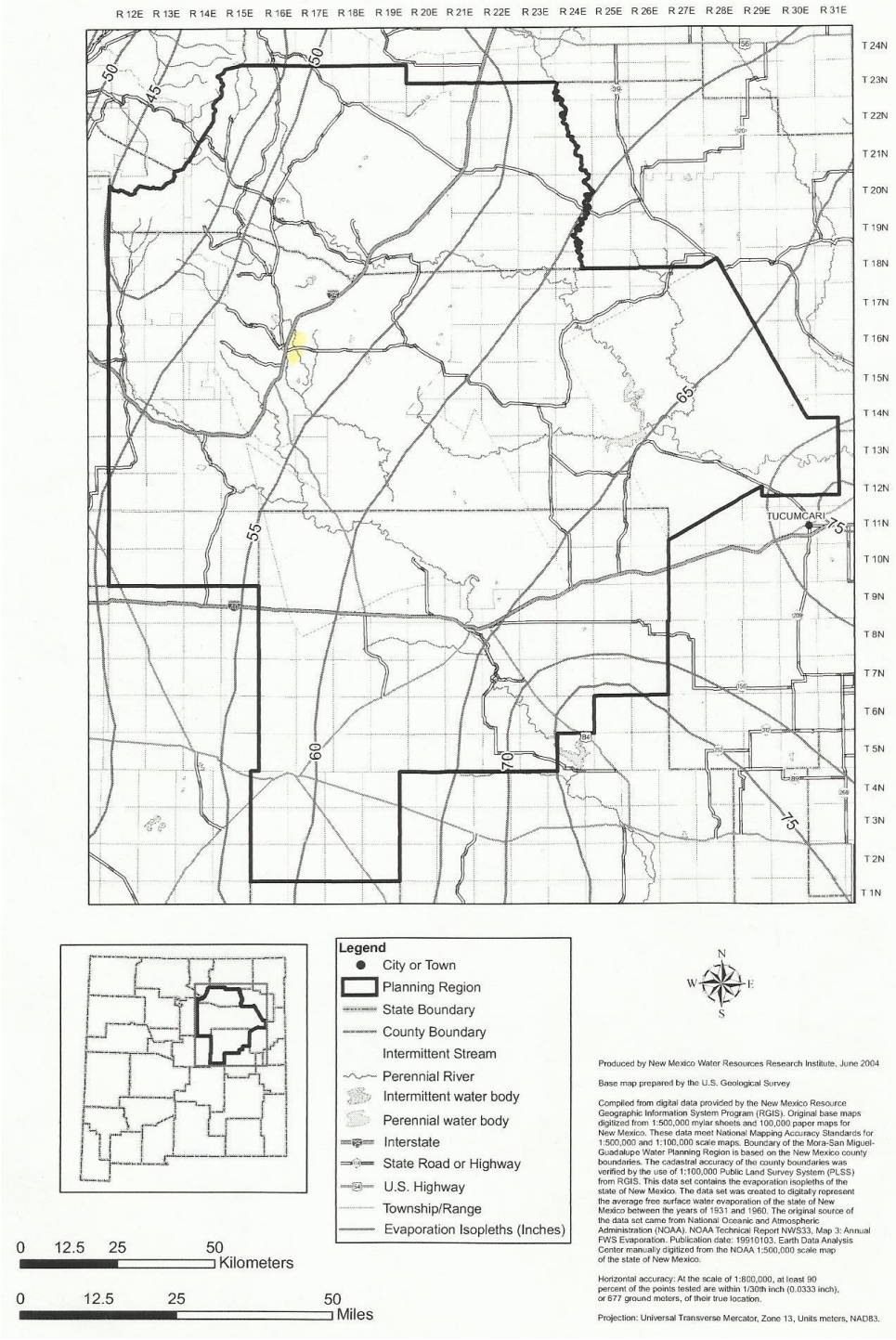

(WRRI, 2004)

APPENDIX D

DESIGNATED NEW MEXICO GROUNDWATER BASINS

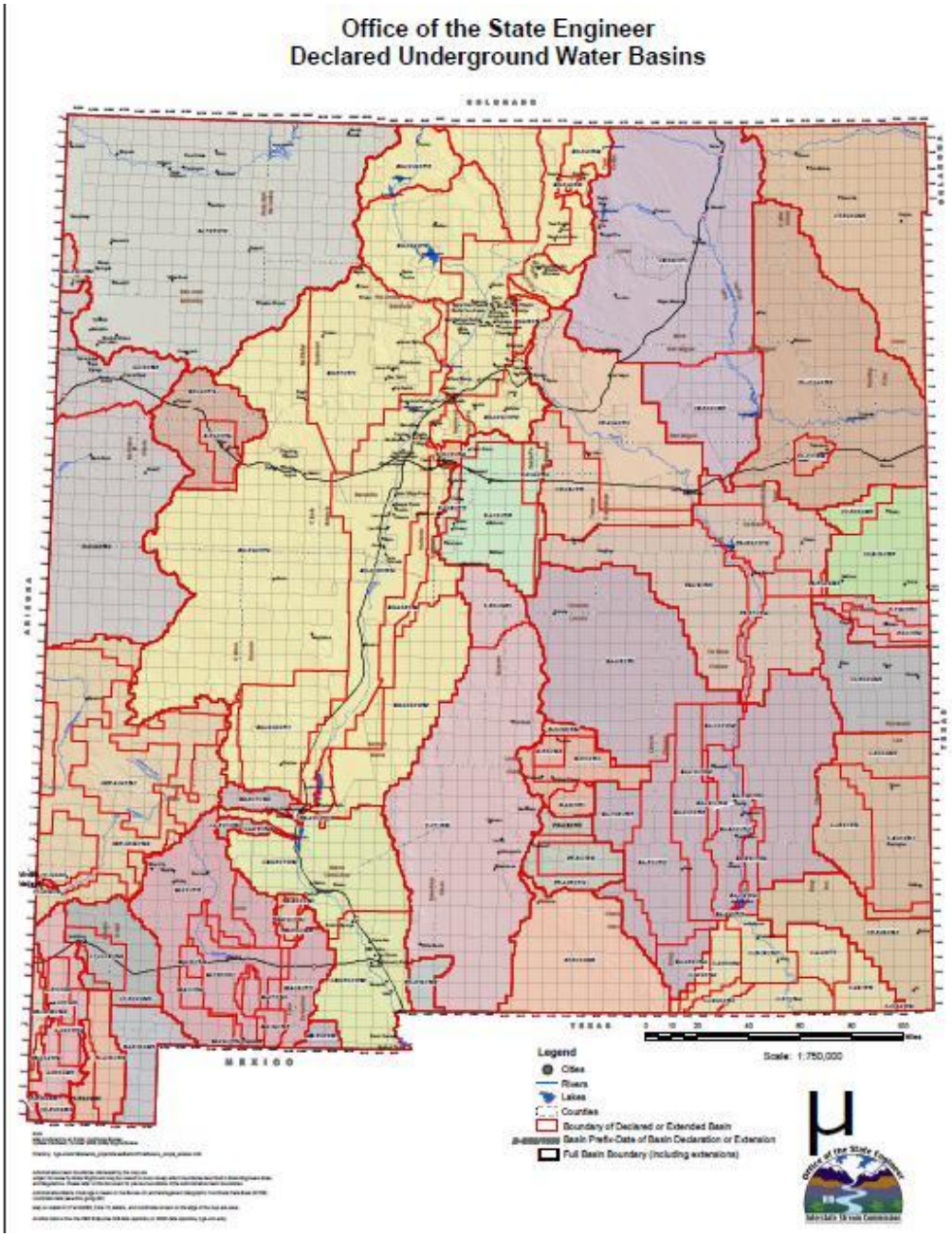
Office of the State Engineer
Declared Underground Water Basins
COLORADO
ARIZONA
NEW MEXICO
TEXAS
MEXICO
Legend
Cities
Rivers
Lakes
Counties
Boundary of Declared or Extended Basin
Basin Prefix-Date of Basin Declaration or Extension
Full Basin Boundary (including extensions)
Scale: 1:750,000

APPENDIX E

ADDITIONAL CHEMICAL DATA

local sample	Sampling	Sample	ppm	ppm	ppm	ppm	ppm	ppm	ppm
ID for easy	Site	Location	F	Cl	NO_2	Br	NO_3	PO_4	SO_4
tracking									
DI water	UTA Lab	UTA lab Milipore		0.051			0.038		
IGR-2	Montezuma	Gallinas River	0.681	5.62	<0.100	<0.100	0.045	<0.100	10.9
IM-2	Montezuma	Montezuma Hot Springs	22	178	<0.100	0.846	0.094	<0.100	40.6
IDGR-2	Milliken Ranch	Devil's Gulch Ravine	0.052	2.17	<0.100	<0.100	0.138	<0.100	6.37
IGW-2	Milliken Ranch	Generator Well	0.512	10.2	<0.100	<0.100	0.762	<0.100	225
ITW-2	Milliken Ranch	Top Well	0.393	8.69	<0.100	<0.100	0.904	<0.100	30.7
IFW-2	Milliken Ranch	Fork Well	0.440	16.6	<0.100	<0.100	3.14	<0.100	108
ITMW-2	Taylor Ranch	Taylor Well	0.328	13.4	<0.100	<0.100	0.311	<0.100	64.3
IDGW-2	Milliken Ranch	Devil's Gulch Well	0.225	7.72	<0.100	<0.100	0.505	<0.100	94.5
IDGP-2	Milliken Ranch	Devil's Gulch Pond	0.108	4.34	<0.100	<0.100	0.311	<0.100	2.01
IMB-2	Milliken Ranch	Milliken Barn Well	0.303	9.25	<0.100	<0.100	0.515	<0.100	62.9
IPR-2	LV Water	Peterson Reservoir	0.170	1.36	<0.100	<0.100	0.069	<0.100	6.07
IBR-2	LV Water	Bradner Reservoir	0.361	2.83	<0.100	<0.100	0.082	<0.100	13.2
IGRII-2	Montezuma	Gallinas River	0.308	3.25	<0.100	<0.100	0.020	<0.100	6.13

local sample	Sampling	Sample	total inorganic carbon		non-purgeable organic carbon			HCO_3
ID for easy	Site	Location			average	SD		
tracking			(ppm)		(ppm)	(ppm)		
DI water	UTA Lab	UTA lab Milipore	0		0.665	0.030		0
IGR-2	Montezuma	Gallinas River	43.6		2.00	0.037		222
IM-2	Montezuma	Montezuma Hot Springs	36.8		0.337	0.007		187
IDGR-2	Milliken Ranch	Devil's Gulch Ravine	11.3		2.80	0.023		57.5
IGW-2	Milliken Ranch	Generator Well	106		0.486	0.006		538
ITW-2	Milliken Ranch	Top Well	117		0.000	0.000		594
IFW-2	Milliken Ranch	Fork Well	223		1.58	0.187		1132
ITMW-2	Taylor Ranch	Taylor Well	128		0.000	0.000		650
IDGW-2	Milliken Ranch	Devil's Gulch Well	102		1.58	0.008		520
IDGP-2	Milliken Ranch	Devil's Gulch Pond	27.4		3.01	0.001		139
IMB-2	Milliken Ranch	Milliken Barn Well	117		0.186	0.028		593
IPR-2	LV Water	Peterson Reservoir	27.0		0.694	0.148		137
IBR-2	LV Water	Bradner Reservoir	36.5		1.16	0.004		186
IGRII-2	Montezuma	Gallinas River	28.8		1.42	0.040		146

local sample ID for easy tracking	Na (ppb)	Mg (ppb)	Si (ppb)	K (ppb)	Ca (ppb)
DI water	780	14	516	357	1745
IGR-3	6357	2569	3066	682	29559
IM-3	166897	130	31926	3943	3769
IDGR-3	2809	1568	1642	1109	19046
IGW-3	20228	22896	8113	1405	99923
ITW-3	12985	7489	5850	1123	71675
IFW-3	18985	23662	8004	1203	68183
ITMW-3	91875	16412	5663	1014	38895
IDGW-3	23326	23892	7666	1521	72039
IDGP-3	3043	2092	854	8321	13413
IMB-3	23607	23901	7114	1498	75312
IPR-3	1498	1537	2327	308	16985
IBR-3	4812	3922	530	700	21354
IGRII-3	2917	1727	3069	1315	19349
IGR-4	6702	2660	3453	946	31008
IM-4	164810	93	30487	3881	3708
IDGR-4	1375	1227	1741	822	18621
IGW-4	21313	24093	8220	1448	107067
ITW-4	12914	7505	5827	1054	71497
IFW-4	19630	24028	8353	1226	72047
ITMW-4	90937	15501	5520	1004	39137
IDGW-4	23211	23796	9087	1405	73240
IDGP-4	2004	2065	1050	7525	13755
IMB-4	23205	23502	6912	1493	75136
IPR-4	1647	1638	2549	406	17917
IBR-4	4670	3927	530	571	21603

local sample ID for easy tracking	Li (ppb)	Be (ppb)	B (ppb)	Al (ppb)	Ti (ppb)	V (ppb)
DI water	0.065	0.126	3.34	14.3	0.249	0.175
IGR-3	10.2	0.087	12.8	67.9	1.93	0.110
IM-3	405	0.099	530	42.3	7.34	1.48
IDGR-3	0.750	0.114	4.83	82.2	2.89	0.480
IGW-3	25.3	0.089	44.9	23.4	2.32	2.90
ITW-3	25.9	0.091	38.0	39.6	2.15	0.081
IFW-3	21.8	0.086	34.5	21.6	2.74	1.59
ITMW-3	65.4	0.070	115	55.5	2.12	0.950
IDGW-3	25.1	0.075	35.9	22.4	2.63	1.32
IDGP-3	1.60	0.441	22.6	924	2.75	7.89
IMB-3	27.0	0.099	41.5	28.3	1.94	0.195
IPR-3	2.36	0.108	7.14	112	1.46	0.145
IBR-3	4.75	0.087	9.64	44.5	0.421	0.286
IGRII-3	67.6	0.109	119	41.3	1.72	1.10
IGR-4	10.9	0.149	14.6	173	2.53	0.217
IM-4	412	0.177	518	88.2	6.62	1.17
IDGR-4	0.605	0.236	2.83	619	2.75	1.22
IGW-4	26.0	0.098	48.3	27.8	2.34	3.08
ITW-4	26.2	0.084	40.1	20.8	1.64	0.053
IFW-4	23.7	0.177	38.4	29.8	2.94	1.94
ITMW-4	28.2	0.061	41.3	34.8	2.30	0.288
IDGW-4	1.29	0.096	22.4	173	2.96	0.470
IDGP-4	26.1	0.085	42.0	25.1	1.91	0.192
IMB-4	14.9	0.084	23.0	103	1.88	0.265
IPR-4	5.15	0.115	9.98	37.0	1.94	0.208
IBR-4	7.07	0.098	8.86	29.5	0.718	0.277

local sample ID for easy tracking	Cr (ppb)	Fe (ppb)	Mn (ppb)	Co (ppb)	Ni (ppb)	Cu (ppb)
DI water	<0.01	1.78	0.162	0.051	0.972	2.94
IGR-3	0.085	430	13.3	0.124	2.47	8.17
IM-3	0.437	46.2	1.14	0.040	0.799	6.69
IDGR-3	0.578	197	1.94	0.274	4.60	15.9
IGW-3	0.282	1262	1.65	0.167	3.85	9.01
ITW-3	0.046	1421	25.5	0.284	2.78	4.75
IFW-3	0.239	1148	5.92	0.120	2.74	4.46
ITMW-3	1.65	392	5.01	0.318	4.66	11.3
IDGW-3	0.723	9072	68.6	0.294	4.34	16.4
IDGP-3	0.733	2922	223	2.43	8.65	36.6
IMB-3	0.694	1446	65.9	0.570	4.07	7.64
IPR-3	0.305	258	13.7	0.160	3.69	21.8
IBR-3	0.271	232	3.81	0.095	2.70	16.8
IGRII-3	0.878	433	4.24	0.278	3.04	13.0
IGR-4	0.056	586	23.7	0.157	2.05	4.87
IM-4	0.983	64.7	1.64	0.054	0.627	16.6
IDGR-4	0.970	598	7.54	0.415	4.34	17.7
IGW-4	0.618	1209	1.39	0.188	5.39	21.7
ITW-4	1.03	1431	25.7	0.262	2.92	7.37
IFW-4	0.899	1192	6.75	0.145	2.99	4.17
ITMW-4	0.653	945	44.1	0.240	25.0	7.45
IDGW-4	5.29	209	112	1.02	13.20	53.7
IDGP-4	0.724	1018	69.3	0.553	3.96	6.84
IMB-4	0.547	1097	34.2	0.350	8.04	13.0
IPR-4	1.18	200	0.652	0.068	3.38	20.7
IBR-4	2.18	181	5.85	0.366	18.3	9.69

local sample ID for easy tracking	Zn (ppb)	Ga (ppb)	Ge (ppb)	As (ppb)	Br (ppb)	Se (ppb)
DI water	2.55	0.030	0.118	0.217	0.407	0.424
IGR-3	10.7	0.055	0.286	0.363	0.412	0.435
IM-3	4.82	2.00	8.33	3.23	0.700	2.78
IDGR-3	23.6	0.040	0.134	0.448	0.399	0.424
IGW-3	184	0.019	0.397	0.924	0.415	2.57
ITW-3	27.9	0.025	0.308	0.282	0.400	0.503
IFW-3	16.1	0.020	0.295	0.649	0.374	2.91
ITMW-3	28.4	0.031	0.307	2.01	0.417	2.39
IDGW-3	33.4	0.042	1.68	0.264	0.387	0.508
IDGP-3	27.0	0.245	0.579	1.67	0.348	0.386
IMB-3	8.34	0.043	0.375	0.214	0.389	1.24
IPR-3	23.3	0.100	0.126	0.264	0.360	0.446
IBR-3	11.1	0.033	0.121	0.480	0.345	0.384
IGRII-3	29.8	0.302	0.294	2.18	0.371	2.16
IGR-4	19.6	1.13	0.426	0.363	0.412	0.451
IM-4	11.1	2.88	8.36	2.95	0.661	2.20
IDGR-4	110	0.136	0.187	0.473	0.376	0.446
IGW-4	222	0.025	0.388	0.940	0.410	2.35
ITW-4	29.6	0.028	0.288	0.282	0.389	0.523
IFW-4	27.6	0.095	0.277	0.728	0.398	2.93
ITMW-4	4.13	0.019	0.250	0.222	0.407	0.985
IDGW-4	8.56	0.054	0.137	1.08	0.356	0.400
IDGP-4	7.29	0.023	0.313	0.216	0.403	1.33
IMB-4	4.59	0.057	0.292	0.270	0.365	1.21
IPR-4	8.54	0.020	0.103	0.476	0.351	0.387
IBR-4	4.05	0.051	0.168	0.277	0.358	0.426

local sample ID for easy tracking	Rb (ppb)	Sr (ppb)	Y (ppb)	Zr (ppb)	Nb (ppb)	Mo (ppb)
DI water	0.053	0.389	0.019	0.228	0.280	0.465
IGR-3	1.65	72.5	0.123	0.768	0.136	1.05
IM-3	54.6	97.7	0.038	1.05	0.440	12.2
IDGR-3	0.399	37.2	0.497	4.10	0.068	0.308
IGW-3	1.63	680	0.026	2.25	0.030	1.97
ITW-3	2.26	225	0.511	4.27	0.032	0.673
IFW-3	1.91	291	0.028	2.08	0.023	0.730
ITMW-3	1.12	816	0.046	2.27	0.219	1.91
IDGW-3	0.997	399	0.047	1.17	0.081	0.099
IDGP-3	1.09	37.9	3.43	3.13	0.066	0.251
IMB-3	2.31	501	0.036	1.76	0.046	0.982
IPR-3	0.614	44.0	0.299	2.26	0.035	0.365
IBR-3	0.304	104	0.100	1.84	0.027	0.814
IGRII-3	1.01	801	0.055	0.891	0.395	2.11
IGR-4	2.70	74.4	0.335	0.607	0.091	0.871
IM-4	52.9	99.3	0.083	4.62	0.262	11.6
IDGR-4	0.652	32.1	0.949	2.97	0.050	0.152
IGW-4	1.66	678	0.021	1.05	0.027	1.96
ITW-4	2.31	228	0.023	1.39	0.026	0.666
IFW-4	2.21	308	0.059	1.49	0.425	0.930
ITMW-4	1.06	397	0.010	1.78	0.120	0.696
IDGW-4	1.32	34.2	0.231	1.54	0.082	0.737
IDGP-4	2.33	518	0.015	1.43	0.050	1.01
IMB-4	1.43	274	0.078	4.71	0.042	0.719
IPR-4	0.294	102	0.031	5.64	0.063	0.918
IBR-4	0.770	44.3	0.051	1.11	0.029	0.559

local sample ID for easy tracking	Ru (ppb)	Rh (ppb)	Pd (ppb)	Ag (ppb)	Cd (ppb)	Sn (ppb)
DI water	0.024	0.046	0.356	35.5	0.063	0.091
IGR-3	0.032	0.043	0.255	12.1	0.067	0.106
IM-3	0.021	0.039	0.411	0.087	0.088	0.071
IDGR-3	0.020	0.040	0.638	0.134	0.078	0.079
IGW-3	0.093	0.059	0.365	1.35	0.076	0.178
ITW-3	0.055	0.031	0.598	0.053	0.051	0.098
IFW-3	0.085	0.033	0.363	28.7	0.050	0.061
ITMW-3	0.120	0.059	0.540	0.353	0.127	0.244
IDGW-3	0.065	0.034	0.294	0.072	0.053	0.264
IDGP-3	0.007	0.022	0.598	0.073	0.163	0.100
IMB-3	0.094	0.037	0.336	0.047	0.063	0.102
IPR-3	0.019	0.018	0.372	0.176	0.114	0.257
IBR-3	0.024	0.017	0.329	0.062	0.067	0.087
IGRII-3	0.143	0.063	0.503	0.093	0.065	0.198
IGR-4	0.027	0.035	0.236	31.6	0.083	0.069
IM-4	0.022	0.039	0.748	0.063	0.114	0.224
IDGR-4	0.012	0.028	0.462	0.088	0.148	0.257
IGW-4	0.119	0.058	0.216	0.062	0.097	0.115
ITW-4	0.054	0.031	0.293	0.041	0.061	0.252
IFW-4	0.074	0.054	0.536	0.149	0.081	0.109
ITMW-4	0.087	0.039	0.404	1.06	0.074	0.071
IDGW-4	0.015	0.027	0.431	0.055	0.161	0.159
IDGP-4	0.090	0.040	0.279	0.044	0.075	0.071
IMB-4	0.049	0.027	0.673	0.510	0.049	0.145
IPR-4	0.026	0.020	0.812	0.182	0.049	0.071
IBR-4	0.016	0.015	0.224	0.548	0.411	0.295

local sample ID for easy tracking	Sb (ppb)	I (ppb)	Te (ppb)	Cs (ppb)	Ba (ppb)	La (ppb)
DI water	0.041	0.350	0.041	0.036	1.58	0.034
IGR-3	0.065	0.277	0.050	1.15	24.3	0.153
IM-3	0.190	1.04	0.032	41.0	5.27	0.040
IDGR-3	0.134	0.349	0.015	0.053	20.5	0.291
IGW-3	0.040	1.09	0.006	0.236	36.1	0.100
ITW-3	0.056	0.510	0.031	0.236	63.1	0.062
IFW-3	0.033	0.724	<0.01	0.194	80.7	0.034
ITMW-3	0.261	0.348	<0.01	0.082	48.7	0.225
IDGW-3	0.033	0.562	<0.01	0.041	119	0.068
IDGP-3	0.119	0.442	<0.01	0.036	106	3.80
IMB-3	0.061	0.815	<0.01	0.037	68.1	0.065
IPR-3	0.060	0.189	<0.01	0.093	20.2	0.250
IBR-3	0.076	0.182	<0.01	0.030	46.7	0.103
IGRII-3	0.248	0.766	<0.01	0.100	46.9	0.080
IGR-4	0.058	0.256	0.040	2.52	26.3	0.385
IM-4	0.181	0.983	0.013	40.9	5.65	0.089
IDGR-4	0.123	0.290	0.004	0.063	29.7	0.945
IGW-4	0.049	0.717	0.024	0.119	35.8	0.093
ITW-4	0.051	0.593	<0.01	0.161	63.0	0.070
IFW-4	0.060	0.586	0.010	0.286	84.9	0.073
ITMW-4	0.056	0.752	<0.01	0.044	76.9	0.028
IDGW-4	0.178	0.471	<0.01	0.093	41.0	0.266
IDGP-4	0.057	0.901	<0.01	0.032	68.0	0.053
IMB-4	0.061	0.567	0.010	0.057	44.2	0.087
IPR-4	0.065	0.197	<0.01	0.018	44.9	0.050
IBR-4	0.087	0.204	0.016	0.356	18.4	0.032

local sample ID for easy tracking	Pr (ppb)	Nd (ppb)	Ce (ppb)	Sm (ppb)	Eu (ppb)	Gd (ppb)
DI water	0.020	0.025	0.039	0.024	0.020	0.023
IGR-3	0.037	0.145	0.391	0.051	0.023	0.047
IM-3	0.008	0.021	0.055	0.019	0.007	0.014
IDGR-3	0.091	0.403	0.428	0.121	0.034	0.122
IGW-3	0.007	0.021	0.043	0.033	0.021	0.014
ITW-3	0.014	0.063	0.126	0.077	0.033	0.061
IFW-3	0.007	0.018	0.042	0.059	0.038	0.009
ITMW-3	0.008	0.025	0.069	0.041	0.027	0.013
IDGW-3	0.008	0.037	0.082	0.067	0.053	0.016
IDGP-3	1.13	4.93	7.84	1.03	0.248	1.22
IMB-3	0.007	0.029	0.078	0.050	0.033	0.013
IPR-3	0.063	0.300	0.482	0.077	0.021	0.087
IBR-3	0.028	0.113	0.203	0.061	0.030	0.040
IGRII-3	0.018	0.038	0.049	0.045	0.034	0.024
IGR-4	0.107	0.417	1.29	0.105	0.028	0.122
IM-4	0.015	0.051	0.123	0.022	0.012	0.029
IDGR-4	0.276	1.21	2.29	0.311	0.081	0.360
IGW-4	0.006	0.017	0.044	0.034	0.023	0.013
ITW-4	0.007	0.016	0.051	0.048	0.032	0.012
IFW-4	0.030	0.058	0.102	0.089	0.064	0.041
ITMW-4	0.004	0.019	0.031	0.061	0.039	0.008
IDGW-4	0.055	0.196	0.399	0.071	0.033	0.055
IDGP-4	0.004	0.017	0.036	0.053	0.034	0.010
IMB-4	0.020	0.078	0.147	0.047	0.026	0.028
IPR-4	0.011	0.030	0.072	0.043	0.026	0.018
IBR-4	0.006	0.024	0.036	0.023	0.012	0.011

local sample ID for easy tracking	Tb (ppb)	Dy (ppb)	Ho (ppb)	Er (ppb)	Tm (ppb)	Yb (ppb)
DI water	0.019	0.021	0.017	0.023	0.018	0.021
IGR-3	0.014	0.032	0.011	0.024	0.008	0.026
IM-3	0.006	0.014	0.005	0.011	0.005	0.009
IDGR-3	0.024	0.094	0.024	0.057	0.011	0.057
IGW-3	0.005	0.009	0.004	0.009	0.005	0.010
ITW-3	0.016	0.077	0.015	0.038	0.008	0.051
IFW-3	0.004	0.011	0.004	0.007	0.004	0.006
ITMW-3	0.013	0.010	0.006	0.012	0.005	0.009
IDGW-3	0.005	0.013	0.005	0.011	0.003	0.009
IDGP-3	0.167	0.827	0.151	0.391	0.050	0.330
IMB-3	0.006	0.010	0.004	0.008	0.003	0.008
IPR-3	0.016	0.064	0.015	0.034	0.006	0.032
IBR-3	0.007	0.022	0.005	0.015	0.003	0.011
IGRII-3	0.013	0.021	0.014	0.021	0.012	0.018
IGR-4	0.022	0.087	0.018	0.051	0.012	0.042
IM-4	0.011	0.022	0.007	0.018	0.006	0.018
IDGR-4	0.050	0.255	0.048	0.127	0.019	0.122
IGW-4	0.005	0.007	0.005	0.010	0.003	0.008
ITW-4	0.004	0.011	0.004	0.009	0.003	0.009
IFW-4	0.027	0.029	0.024	0.032	0.022	0.029
ITMW-4	0.003	0.007	0.003	0.007	0.004	0.009
IDGW-4	0.010	0.042	0.008	0.026	0.005	0.023
IDGP-4	0.005	0.006	0.003	0.007	0.003	0.007
IMB-4	0.006	0.018	0.005	0.012	0.004	0.013
IPR-4	0.005	0.013	0.004	0.010	0.003	0.009
IBR-4	0.004	0.011	0.005	0.012	0.004	0.015

local sample ID for easy tracking	Lu (ppb)	Hf (ppb)	Ta (ppb)	W (ppb)	Re (ppb)
DI water	0.018	0.083	0.301	0.370	0.370
IGR-3	0.008	0.091	0.324	2.77	0.358
IM-3	0.004	0.254	3.92	174	0.698
IDGR-3	0.013	0.258	0.139	0.749	0.549
IGW-3	0.004	0.119	0.155	0.776	0.434
ITW-3	0.009	0.225	0.082	0.275	0.397
IFW-3	0.004	0.123	0.085	0.454	0.369
ITMW-3	0.005	0.197	0.386	0.509	0.415
IDGW-3	0.003	0.087	0.180	0.149	0.393
IDGP-3	0.049	0.247	0.091	0.130	0.379
IMB-3	0.003	0.104	0.103	0.313	0.392
IPR-3	0.007	0.126	0.069	0.131	0.378
IBR-3	0.004	0.089	0.068	0.126	0.361
IGRII-3	0.014	0.183	0.551	0.445	0.406
IGR-4	0.012	0.078	0.250	2.21	0.385
IM-4	0.008	0.369	2.50	167	0.384
IDGR-4	0.019	0.209	0.089	0.389	0.360
IGW-4	0.005	0.059	0.142	0.766	0.458
ITW-4	0.004	0.093	0.081	0.317	0.400
IFW-4	0.025	0.191	0.492	0.699	0.450
ITMW-4	0.004	0.126	0.322	0.246	0.429
IDGW-4	0.005	0.166	0.135	0.419	0.378
IDGP-4	0.004	0.079	0.125	0.307	0.385
IMB-4	0.004	0.312	0.086	0.220	0.415
IPR-4	0.003	0.321	0.083	0.198	0.392
IBR-4	0.004	0.088	0.102	1.28	0.330

local sample ID for easy tracking	Ir (ppb)	Pt (ppb)	Au (ppb)	Hg (ppb)	Tl (ppb)
DI water	0.170	0.038	0.248	0.679	0.115
IGR-3	0.212	0.029	0.483	0.485	0.079
IM-3	0.216	0.017	1.26	7.10	0.171
IDGR-3	0.222	0.022	0.147	0.255	0.049
IGW-3	0.169	0.019	0.225	0.236	0.040
ITW-3	0.133	0.018	0.171	0.247	0.049
IFW-3	0.101	0.015	0.200	0.207	0.035
ITMW-3	0.165	2.37	0.609	0.376	0.055
IDGW-3	0.114	0.018	0.223	0.240	0.037
IDGP-3	0.102	0.016	0.170	0.189	0.030
IMB-3	0.097	0.016	0.183	0.189	0.101
IPR-3	0.070	0.020	0.085	0.159	0.021
IBR-3	0.064	0.011	0.096	0.121	0.017
IGRII-3	0.150	0.026	0.914	0.585	0.085
IGR-4	0.153	0.025	0.396	0.379	0.072
IM-4	0.204	0.022	0.914	6.40	0.188
IDGR-4	0.141	0.022	0.147	0.228	0.049
IGW-4	0.172	0.017	0.206	0.236	0.038
ITW-4	0.117	0.014	0.172	0.198	0.041
IFW-4	0.192	0.044	0.640	0.648	0.093
ITMW-4	0.134	0.011	0.272	0.294	0.033
IDGW-4	0.115	0.013	0.236	0.211	0.034
IDGP-4	0.100	0.012	0.204	0.193	0.099
IMB-4	0.080	0.014	0.126	0.176	0.065
IPR-4	0.074	0.019	0.111	0.132	0.020
IBR-4	0.068	0.036	0.110	0.179	0.018

local sample ID for easy tracking	Pb (ppb)	Bi (ppb)	Th (ppb)	U (ppb)
DI water	0.269	0.184	0.037	0.486
IGR-3	0.715	0.049	0.042	1.54
IM-3	0.292	0.586	0.071	0.791
IDGR-3	0.616	10.2	0.051	0.756
IGW-3	1.02	3.44	0.020	8.24
ITW-3	0.492	5.37	0.020	2.80
IFW-3	0.472	2.83	0.014	4.86
ITMW-3	1.20	10.5	0.033	5.42
IDGW-3	1.15	5.60	0.028	5.29
IDGP-3	5.97	4.39	0.181	0.841
IMB-3	0.857	4.94	0.019	5.48
IPR-3	1.62	6.10	0.018	0.977
IBR-3	0.743	3.54	0.014	1.32
IGRII-3	1.39	5.77	0.062	5.17
IGR-4	0.974	0.129	0.081	1.60
IM-4	0.968	5.65	0.075	0.546
IDGR-4	3.09	5.94	0.154	0.631
IGW-4	2.05	2.50	0.021	8.78
ITW-4	0.476	7.85	0.017	2.84
IFW-4	0.679	2.95	0.073	5.18
ITMW-4	0.674	3.09	0.018	5.45
IDGW-4	1.02	2.64	0.048	0.689
IDGP-4	0.705	2.58	0.014	5.34
IMB-4	0.673	6.71	0.020	3.38
IPR-4	0.343	11.4	0.049	1.42
IBR-4	0.513	6.77	0.010	0.948

REFERENCES

Abdalla, O. 2009. Groundwater Recharge/Discharge in Semi-arid Regions Interpreted from Isotope and Chloride Concentrations in North White Nile Rift, Sudan. *Hydrogeology Journal*. 17: 679-692.

Aguirre, L. 2009. Water Master Report: Gallinas River. *OSE Interstate Stream Commission Report*. 5-35.

Aji, K., Tang, C., Song, X., Kondoh, A., Sakura, Y., Yu, J. and Kaneko, S. 2008. Characteristics of Chemistry and Stable Isotopes in Groundwater of Chaobai and Yongding River Basin, North China Plain. *Hydrological Processes*. 22: 63 – 72.

Apaydin, A. 2010. Relation of Tectonic Structure to Groundwater Flow in the Beypazari Region, NW Anatolia, Turkey. *Hydrogeology* Journal. 18: 1343 – 1356.

Arnason, B. 1977. Hot Groundwater Systems in Iceland Traced by Deuterium. *Nordic Hydrology*. 8: 93-102.

Baltz, E. and Myers, D. 1999. *Stratigraphic Framework of Upper Paleozoic Rocks, Southeastern Sangre de Cristo Mountains, New Mexico with a Section onSspeculations and Implications for Regional Interpretation of Ancestral Rocky Mountains Paleotectonics*. United States Geological Survey: Socorro, NM.

Barnes, S. and Worden, R.H. 1998. Understanding groundwater sources and movement using water chemistry and tracers in low matrix permeability terrain: the Cretaceous (Chalk) Ulster White Limestone Formation, Northern Ireland. *Applied Geochemistry*. 13: 143 – 153.

Bejnar, W. and Bejnar, K.C. 1979. Structural Geology Related to Montezuma Hot Springs, Montezuma, New Mexico. *New Mexico Geology*. 1: 21 – 24.

Blasch, K. and Bryson, J. 2007. Distinguishing Sources of Ground Water Recharge by Using δ^2H and $\delta^{18}O$. *Ground Water*. Vol. 45, No. 3: 294 – 308.

Bowen, G., Ehleringer, J., Chesson, L., Stange, E. and Cerling, T. 2007. Stable Isotope Ratios of Tap Water in the Contiguous United States. *Water Resources Research*. Vol. 43: WO3419, doi:10.1029/2006WR005186.

Cartwright, A., Weaver, T., and Fifield, L. 2005. Cl/Br Ratios in Environmental Isotopes as Indicators of Recharge Variability in Groundwater Flow: an example from the Southeast Murray basin, Australia. *Chemical Geology*, 31: 38 – 56.

Cartwright, I., Hall, S., Tweed, S. and Leblanc, M. 2009. Geochemical and Isotopic Constraints on the Interaction between Saline Lakes and Groundwater in Southeast Australia. *Hydrogeology Journal*. 17: 1991 – 2004.

City of Las Vegas. 2010. *Water System Evaluation and Preliminary Engineering Report*. http://www.lasvegasnm.gov/water_system_eval_presentation_0920.pdf

Colorado Division of Water Resources. 2011. Ground Water Levels. http://water.state.co.us/groundwater/Pages/HydroGeo.aspx

Craig, H. 1961. Isotopic Variations in Meteoric Waters. *Science*. 133: 1702 – 1703.

Dansgaard, W. 1964. Stable Isotopes in Precipitation. *Tellus* XVI. 4: 436 – 467.

Datta, B., Chakrabarty, D. and Dhar, A. 2009. Simultaneous Identification of Unknown Groundwater Pollution Sources and Estimation of Aquifer Parameters. *Journal of Hydrology*. 376: 48 – 57.

Davisson, M.L., Smith, D.K., Kenneally, J. and Rose, T.P. 1999. Isotope Hydrology of Southern Nevada Groundwater: Stable Isotopes and Radiocarbon. *Water Resources Research*. 35: 279-294.

Eaton, G. 2008. Epeirogeny in the Southern Rocky Mountains Region: Evidence and Origin. *Geosphere*. 4: 764-784.

Eby,N. 2003. *Principles of Environmental Geochemistry*. Brooks Cole, 1st edition.

Environmental Protection Agency. 1983. Sample Preservation. *Methods for Chemical Analysis of Water and Wastes*. EPA-600/4-79-020. U.S.E.P.A., Cincinatti, Ohio.

Evans, T. and Lindline, J. 2004. Water Quality Assessment in the Gallinas Watershed, Las Vegas, NM. http://wrri.nmsu.edu/research/rfp/studentgrants03/reports/evans.pdf

Fan, M., Quade, J., Dettman, D. and DeCelles, P. G. 2011. Widespread Basement Erosion during the late Paleocene-early Eocene in the Laramide Rocky Mountains Inferred from $^{87}Sr/^{86}Sr$ ratios of Freshwater Bivalve Fossils. *GSA Bulletin*. 123: 2069 – 2082.

Folch, A. and Mas-Pla, J. 2008. Hydrogeological Interactions between Fault Zones and Alluvial Aquifers in Regional Flow Systems. *Hydrological Processes*. 22: 3476 – 3487.

Freeze, R.A. and Cherry, J. 1979. *Groundwater*. Prentice-Hall, Inc: Englewood Cliffs, NJ.

Gabora, M and Campana, M.E. 2002. Groundwater Flow, Recharge Rates and Mean Ages in the Roswell Basin, Southeastern New Mexico, United States of America. *University of New Mexico, Water Resources Program*. 29 - 53

Gat, J.R. 1996. Oxygen and Hydrogen Isotopes in the Hydrologic Cycle. *Annual Review Earth Planetary Science*. 24: 225 – 262.

Glorieta Geoscience Inc. 1996. *Pumping Test Results Taylor Well Field 17-day Pumping Test and 27-day Recovery Test.*

Grassi, S., Doveri, M., Cortecci, G., and Amadori, M. 2011. Hydrogeological Study of the Intensely Exploited Aquifer of the Santa Croce Leather-producing District, Tuscany (central Italy). *Hydrogeology Journal*. 19: 671 – 684.

Griggs, R. and Hendrickson, G.E. 1951. *Geology and Ground-Water Resources of San Miguel County, New Mexico.* New Mexico Bureau of Mines and Mineral Resources. Socorro, NM: 1951.

Heaton, R. 1935. *Geology and Water Possibilities of a Portion of the Las Vegas Basin, San Miguel County, New Mexico.*

Hem, J. 1985. *USGS Water Supply Paper 2254: Study and Interpretation of the Chemical Characteristics of Natural Water*. 3rd ed.

Hinkle, S., Kauffman, L., Thomas, MA, Brown, C., McCarthy, K., Eberts, S., Rosen, M. and Katz, B. 2009. Combining Particle-tracking and Geochemical Data to Assess Public Supply Well Vulnerability to Arsenic and Uranium. *Journal of Hydrology*. 376: 132 – 142.

Horn, M. and Timmons, J.M. 2004. Preliminary Geologic Map of the Ojitos Frios Quadrangle, San Miguel County, New Mexico. *NMBGMR Open-file Map Series.*

Hunt, R., Coplen, T., Haas, N., Saad, D. and Borchardt, M. 2005. Investigating Surface Water-well Interaction Using Stable Isotope Ratios of Water. *Journal of Hydrology*. 302: 154 - 172.

IAEA/WMO. 2006. Global Network of Isotopes in Precipitation. The GNIP Database. Accessible at: http://www.iaea.org/water

IAEA. The Essential Role of Isotopes in Studies of Water Resources. *IAEA Bulletin*. 19, 1: 9 – 20.

Kaufman, R.F. 1978. *Land and Water Use Effects on Ground-water Quality in Las Vegas Valley*. U.S. Environmental Protection Agency, San Francisco, CA.

Kaysing, J. 2006. Assessment of Arsenic and Other Groundwater Impairments in the Gallinas Watershed, Las Vegas, NM. Master's Thesis: Highlands University.

Koterba, M., Wilde, F. and Lapham, W. 1995. Ground-water Data-collection Protocols and Procedures for the National Water-quality Assessment Program: Collection and Documentation of Water-quality Samples and Related Data. *U.S. Geological Survey Open File Report 95-399*.

Lakshmanan, E., Kannan, R. and Kumar, M. 2003. Major Ion Chemistry and Identification of Hydrogeochemical Processes of Groundwater in a part of Kancheepuram District, Tamil Nadu, India. *Environmental Geosciences*. 10: 157 – 166.

Lambert, S.J. and Balsley, S.D. 1997. Stable-isotopes of Groundwaters from the Albuquerque, New Mexico, Basin: One Decade Later. *Environmental Geology*. 31: 199 – 204

"Las Vegas, NM: 87701 profile." www.city-data.com. 2010. <http://www.city-data.com/city/Las-Vegas-New-Mexico.html>

Lessard, R.H. and Bejnar, W. 1976. Geology of the Las Vegas Area. *New Mexico Geological Society Guidebook*. 27th field conf.: 103 – 108.

Li, F., Pan, G., Tang, C., Zhang, Q. and Yu, J.. 2008. Recharge Source and Hydrogeochemical Evolution of Shallow Groundwater in a Complex Alluvial Fan System, Southwest of North China Plain. *Environmental Geology*. 55: 1109 – 1122.

Lingjuan, M. 2011. Use of Stable Isotopes to Define Hydrological Processes in the Border Rivers Catchment, Murray-Darling Basin.

Lipman, P. and Mehnert, H. 1975. Late Cenozoic Basaltic Volcanism and Development of the Rio Grande Depression in the Southern Rocky Mountains. *Cenozoic History of the Southern Rocky Mountains*. 144: 119 – 178.

Miller, J., Montgomery, A., and Sutherland, P. 1963. *Geology of Part of the Southern Sangre de Cristo Mountains, New Mexico*. New Mexico Bureau of Mines and Mineral Resources: Socorro, NM.

Milliken, A. 2007. Proposal in Response to Request for Proposals for Wells and/or Ground Water Rights: City of Las Vegas, NM.

Mithas, A.D, Sankar, K. and Imran, A.D. 2011. Major Ion Chemistry and Hydrochemical Studies of Groundwater of Parts of Palar River Basin, Tamil Nadu, India. *Environmental Monitoring Assessment*. 176: 621 – 636.

Mukherjee, A., Frayer, A., and Rowe, H. 2006. Regional-scale Stable
Isotope Signatures of Recharge and Deep Groundwater in the Arsenic Affected Areas of West Bengal India. *Journal of Hydrology*. 334: 151 – 161.

Murray, C. 1943. *Ground-water Conditions near Las Vegas, New Mexico.* Geological Survey, U.S. Department of the Interior.

New Mexico Office of the State Engineer. 2011. New Mexico Water Rights Reporting System: Water Rights Lookup. http://nmwrrs.ose.state.nm.us/nmwrrs/index.html.

O'Sullivan, R. 1974. The Upper Triassic Chinle Formation in North-Central New Mexico. New Mexico Geological Society Handbook. 25: 171 – 173.

Peakbagger.com, 2011. Southern Rocky Mountains: Ranges – North America – Rocky Mountains. http://www.peakbagger.com/range.aspx?rid=146

Petitta, M., Primavera, P., Tuccimei, P. and Aravena, R. 2011. Interaction between Deep and Shallow Groundwater Systems in Areas Affected by Quaternary Tectonics (Central Italy): a Geochemical and Isotope Approach. *Environmental Earth Science*. 63: 11 – 30.

Shomaker, J. 2007. *Summary of Information Relating to Wells, Pumping Tests and Water Quality High-Yield Wells on Milliken Ranch Las Vegas, NM*.

Spiegel, S. and Black and Veatch. *Report on Development of Additional Groundwater Supply (Taylor Well Field) Las Vegas, NM*.

Sundance Specialists, Ltd. A. Analysis of Potential 6-Acre Well (UP-3732) Pumping Interference with McCoy Well(UP-2503).

Sundance Specialists, Ltd. B. Preliminary Analysis of the Groundwater Hydraulics of the Taylor Well with Emphasis on TWF #4 and TWF #7.

Tweed, S., Leblanc, M. and Cartwright, I. 2009. Groundwater-surface Water Interaction and the Impact of a Multi-year Drought on Lake conditions in South-East Australia. *Journal of Hydrology*. 379: 41 – 53.

Tweto, O. 1975. Laramide (Late Cretaceous-Early Tertiary) Orogeny in the Southern Rocky Mountains. *Cenozoic History of the Southern Rocky Mountains. 144:* 1-44.

USGS. 2011. Ground Water Quality. USGS Publications, 2011. <http://pubs.usgs.gov/wri/wri024045/htms/report2.htm>

Van Wyk, E, van Tonder, GJ, and Vermeulen, D. 2011. Characteristics of Local Groundwater Recharge Cycles in South African Semi-arid Hard Rock Terrains – Rainwater Input. *Water SA*. 37: 147 – 154.

Wahi, A., Hogan, J., Ekwurzel, B., Baillie, M., and Eastoe, C. 2008. Geochemical Quantification of Semi-arid Mountain Recharge. *Ground Water.* 46, 3: 414 – 425.

WRRI. 2004. Water Resources Research Institute. Fig_7_surface_evaporation.pdf. http://river.nmsu.edu/isc/morasanmiguel/fig7_surface_evaporation/fig7_surface_evaporationb.pdf

White, D.E., Barnes, I., and O'Neil, J.R. 1973. Thermal and Mineral Waters of Nonmeteoric Origin, California Coast Ranges. *Geological Society of America Bulletin*. 84: 547 – 560.

Winograd, I. and Friedman, I. 1972. Deuterium as a Tracer of Regional Ground-Water Flow, Southern Great Basin, Nevada and California. *Geological Society of America Bulletin*. 83: 3691 – 3708.

Yapp, C.J. 1985. D/H Variations of Meteoric Waters in Albuquerque, New Mexico, U.S.A. *Journal of Hydrology*. 76: 63 – 84.

Yidana, S., Banoeng-Yakubo, B., Akabzaa, T. and Asiedu, D. 2011. Characterization of the Groundwater Flow Regime and Hydrochemistry of Groundwater from the Buem Formation, Eastern Ghana. *Hydrological Processes*. 25: 2288 – 2301.

Yuan, R., Song, X., Zhang, Y., Han, D., Wang, S. and Tang, C. 2011. Using Major Ions and Stable Isotopes to Characterize Recharge Regime of a Fault-influenced Aquifer in Beiyishui River Watershed, North China Plain. *Journal of Hydrology*. 405: 512 – 521.

Zhou, X., Fang, B., Zhou H., Li, J. and Wang, Y. 2009. Isotopes of Deuterium and Oxygen-18 in Thermal Groundwater in China. *Environmental Geology*. 57: 1807 – 1814.

BIOGRAPHICAL INFORMATION

Ian Hamilton began his academic career in science while taking his senior year of high school at Clarkson University in Potsdam, NY. He began a major in Cell/Molecular Biology there and continued with the program at Tulane University after receiving a Distinguished Scholar's Award to attend the New Orleans university. Four years later, Ian received a B.S. in Cell/Molecular Biology with an additional dual degree award of a B.A. in Spanish. Several years in the workforce prodded him to return to graduate school with a focus in geology. He attended the University of Texas at Arlington for his graduate studies and received support in the form of the Wanda Schlagle Field Scholarship, a UTA teaching assistantship and the Marathon Oil Geology Scholarship. Ian also took advantage of external educational opportunities at seminars/camps at the University of Minnesota, Midland College Petroleum Professional Development Center and meetings sponsored by the American Association of Petroleum Geologists and the Association of Environmental and Engineering Geologists.

While Ian has worked as a project manager, an educator, and a field geologist, he plans to pursue opportunities that allow him to utilize his interest in geology. The topic of his thesis centered on hydrogeology, and he seeks to gain employment doing environmental remediation and aquifer characterization.